IEEE Access
Multidisciplinary | Rapid Review | Open Access Journal

Received April 14, 2020, accepted April 29, 2020, date of publication May 6, 2020, date of current version May 19, 2020.

Digital Object Identifier 10.1109/ACCESS.2020.2992718

Thermal Analysis in Electromagnetic Rail Launcher Taking Friction Heat into Account Under Active Cooling Condition

XIAOBO WAN[1], JUNYONG LU[2], DELIANG LIANG[1], AND JIANYONG LOU[1]
[1]State Key Laboratory of Electrical Insulation and Power Equipment, School of Electrical Engineering, Xi'an Jiaotong University, Xi'an 710049, China
[2]School of Electrical Engineering, Naval University of Engineering, Wuhan 430033, China

Corresponding author: Jianyong Lou (jylou@mail.xjtu.edu.cn)

This work was supported in part by the National Key Basic Research Program 973 Project of China under Grant 613262, and in part by the National Natural Science Foundation of China under Grant 51737010, Grant 51522706, and Grant 51407191.

ABSTRACT A high-efficiency thermal management system is one of the key points in the practical application of electromagnetic rail launcher (ERL). In this paper, the thermal characteristics in ERL with the section of rectangle, convex, and concave rails by active cooling under different friction coefficient condition are investigated. By two cooling approaches, at two launch rates, with four friction coefficients, peak temperature in convex rails at the same moment is minimum in three types rails. Joule heat dominates in three shapes rail by channel or surface/channel cooling approach, but friction heat is a nonnegligible part under multiple launching mode. The spatial and temporal distribution features of peak temperature of three shapes rail with different friction coefficient under active cooling condition are compared. The mathematical relations between friction coefficient, time and temperature rising caused by friction at pulse end time and shot end moment in ERL with the three types rail are obtained, respectively. In terms of obtaining lower maximal temperature in rail, the ERL with convex rails is the best one.

INDEX TERMS Thermal analysis, electromagnetic rail launcher, friction heat, active cooling.

I. INTRODUCTION

The electromagnetic launching technology has the advantages of high launch efficiency, large launching mass range, high muzzle speed, and good controllability, and is widely believed to be an advanced mode in military and civil areas such as aircraft launch [1], space launch [2]–[5], electromagnetic launcher [6]–[11], and so forth. However, it still has some technical bottlenecks such as ablation and gouging on rail surface. Wetz *et al.* tried to control bore ablation by using magnetic augmentation, synchronously driven distributed power supply, high-purity alumina insulators, and pre-acceleration [12]. Xu *et al*. measured surface resistivity and surface flashover voltage under different ablation areas [13]. Zhang *et al*. analyzed the causes of the transition ablation, proposed corresponding improvement measures and verified them through experiments [14]. Tang *et al.* found that thermal stress concentration is an important cause of gouging [15].The steep temperature rise caused by the extremely large current (MA grade) flowing through rails and armature in very short time (ms grade) is one of the main reasons of erosion and gouging. Hence, efficient thermal management in ERL is a key technology in practical ERL system. Active cooling is an effective thermal management approach in it [6], [7].

In previous studies, plenty of literatures have investigated rail heating and cooling by experiments or simulations. Fish *et al.* analyzed heat distribution characteristics between multiple shots without and with active cooling conditions in rails by finite element code EMAP3D (Electro-Mechanical Analysis Program in 3 Dimension) [16]. Motes *et al.* revealed that Joule heat was the dominant source of heat in rail during launch process under single shot mode by simulations and experiments [17].

During practical launching process, there is friction between rails and sliding armature. Joule heat is the main source of heat in rails during launch process, but it is still necessary to take friction heat into account to reveal spatial and temporal distribution of heat in rail more precisely. After obtaining more exact temperature distribution, more effective

The associate editor coordinating the review of this manuscript and approving it for publication was Jenny Mahoney.

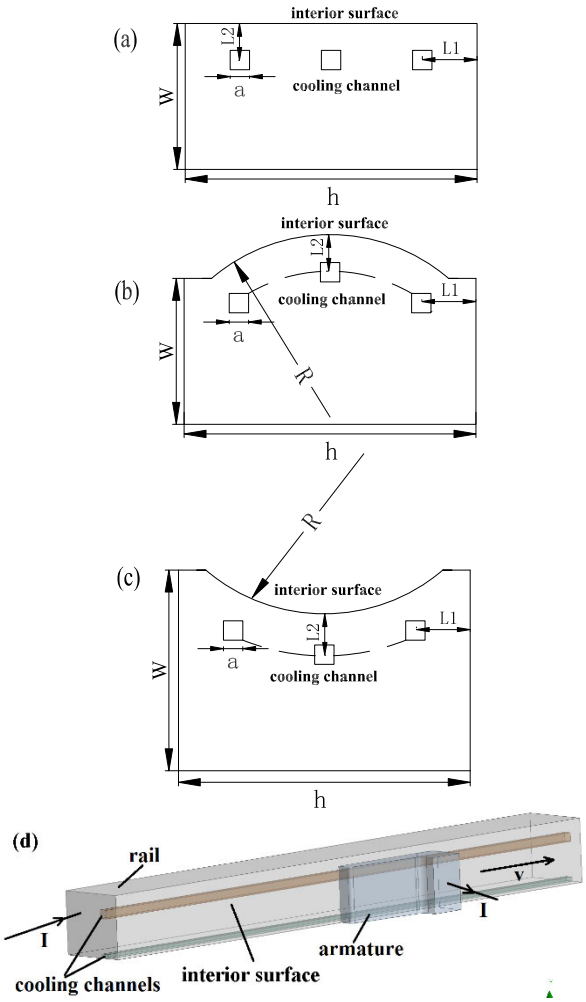

FIGURE 1. Model of ERL with different section rails and cooling channels. (a)Rectangle. (b)Convex. (c)Concave. (d)A quarter model of ERL with rectangle rail and cooling channels.

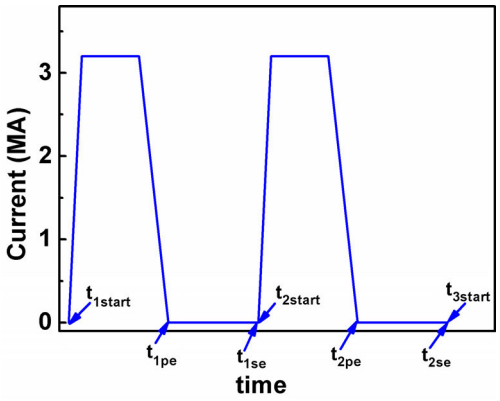

FIGURE 2. Applied pulse waveform.

thermal management strategy can be proposed. Li *et al.* found that friction heat accumulated in the thin layer of interface between armature and rail [18]. A lumped evaluation model and sliding electrical contact mechanism considering friction

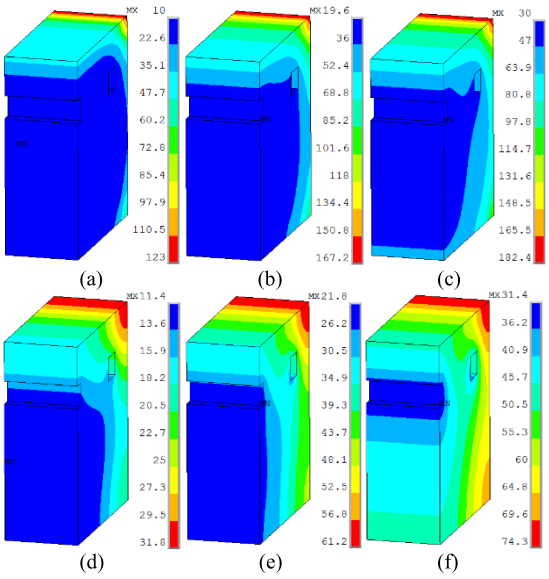

FIGURE 3. Spatial and temporal distribution of temperature near breech in rectangle rail, 10 shots/min, channel cooling, without friction [23]. (a) t_{1pe}. (b) t_{5pe}. (c) t_{10pe}. (d) t_{1se}. (e) t_{5se}. (f) t_{10se}.

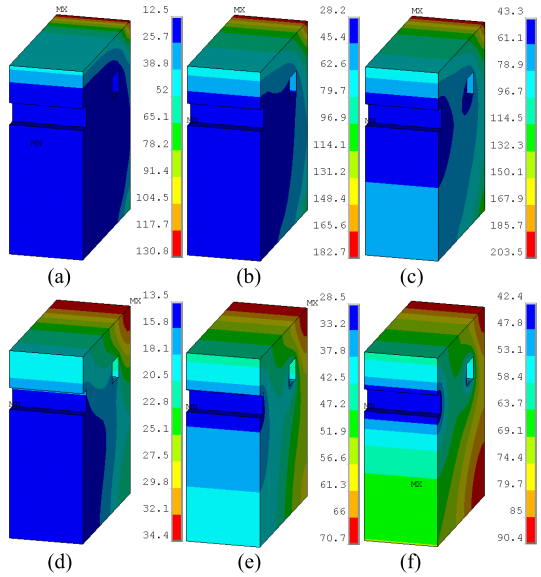

FIGURE 4. Spatial and temporal distribution of temperature near breech in rectangle rail, 10 shots/min, channel cooling, friction coefficient 0.04. (a) t_{1pe}. (b) t_{5pe}. (c) t_{10pe}. (d) t_{1se}. (e) t_{5se}. (f) t_{10se}.

in ERL is established [19], [20]. In terms of section shape, major categories of rails in ERL include rectangle, convex, and concave [21]. Shvetsov *et al.* studied Joule heat in ERL with different copper rails [22]. Wan *et al.* compared thermal features in rectangle, convex, and concave rails under active cooling condition without friction [23]. Nevertheless, these papers did not consider the effect of friction between armature and the three type rails. Besides, there are few literatures about thermal characteristics in ERL with different types rail by active cooling condition with different friction

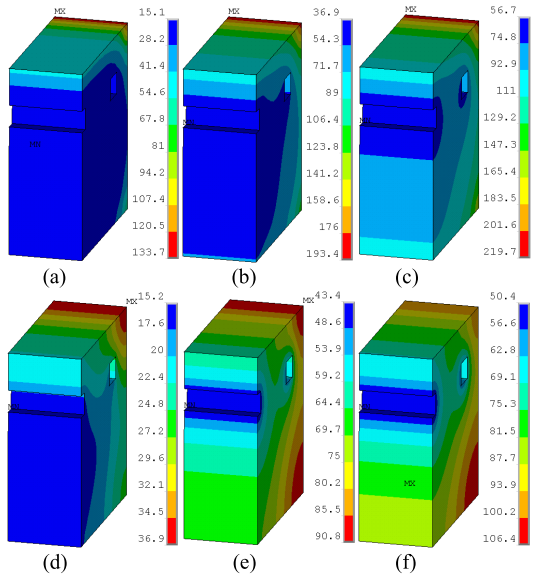

FIGURE 5. Spatial and temporal distribution of temperature near breech in rectangle rail, 10 shots/min, channel cooling, friction coefficient 0.08. (a) t_{1pe}. (b) t_{5pe}. (c) t_{10pe}. (d) t_{1se}. (e) t_{7se}. (f) t_{9se}.

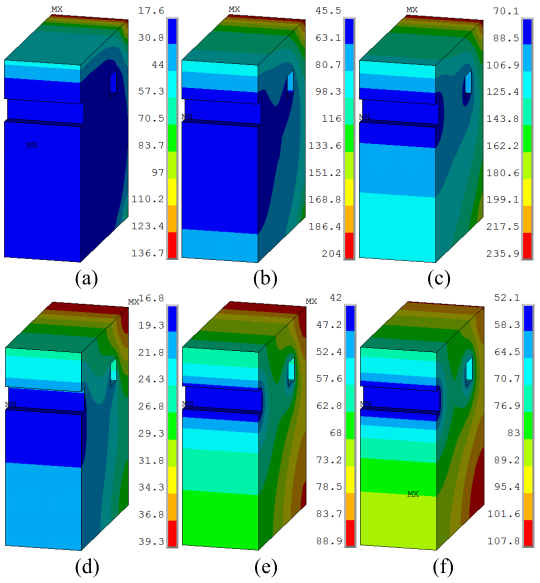

FIGURE 6. Spatial and temporal distribution of temperature near breech in rectangle rail, 10 shots/min, channel cooling, friction coefficient 0.12. (a) t_{1pe}. (b) t_{5pe}. (c) t_{10pe}. (d) t_{1se}. (e) t_{5se}. (f) t_{7se}.

coefficient. Specially, the spatial and temporal distribution of peak temperature under different friction coefficient and the mathematical relations among temperature rising induced by friction in rails, friction coefficient, and time, in multi-shot launch process, have not been reported. Hence, this paper focuses on the above aspects.

II. MODEL OF ERL AND PULSE WAVEFORM

Fig. 1(a) ∼ (c) illustrate section of rectangle, convex, and concave rail with square cooling channels, respectively. a represents square length, h represents rail height, w means

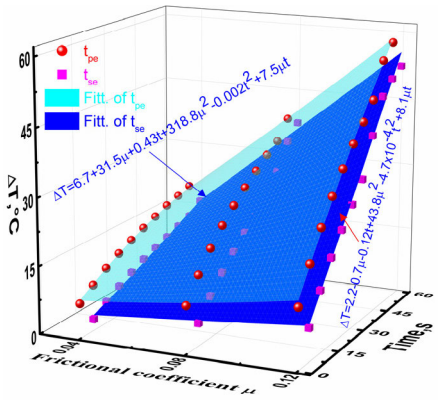

FIGURE 7. Temperature rising caused by friction at t_{pe} and t_{se} in rectangle rails near breech during multi-shot process, by channel cooling, 10 shots/min.

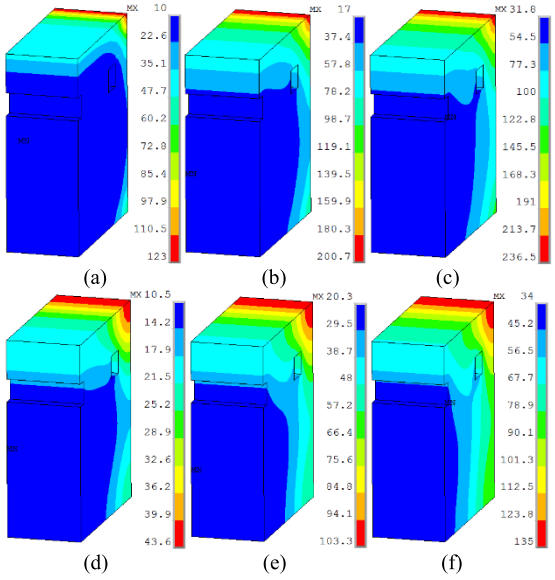

FIGURE 8. Spatial and temporal distribution of temperature near breech in rectangle rail, 20 shots/min, channel cooling, without friction [23]. (a) t_{1pe}. (b) t_{5pe}. (c) t_{10pe}. (d) t_{1se}. (e) t_{5se}. (f) t_{10se}.

TABLE 1. Parameter of different section rails.

Rail type	h(mm)	L_1(mm)	L_2(mm)	a(mm)	W(mm)	R(mm)
Rectangle	160	25	23	10	90	/
Convex	160	25	23	10	79.1	100
Concave	160	25	23	10	92.4	100

rail thickness, R denotes the radius, L_1 represents distance between rail upper/lower surface and cooling channel center, and L_2 is the distance between rail interior surface and cooling channel center. Fig. 1(d) depicts a quarter ERL model with rectangle rail and cooling channels. The air domain surrounding ERL is not given. The models of other two types ERL are similar with it.

To compare the thermal properties under identical conditions, the section area, a, h, R, L_1, and L_2 are kept constant.

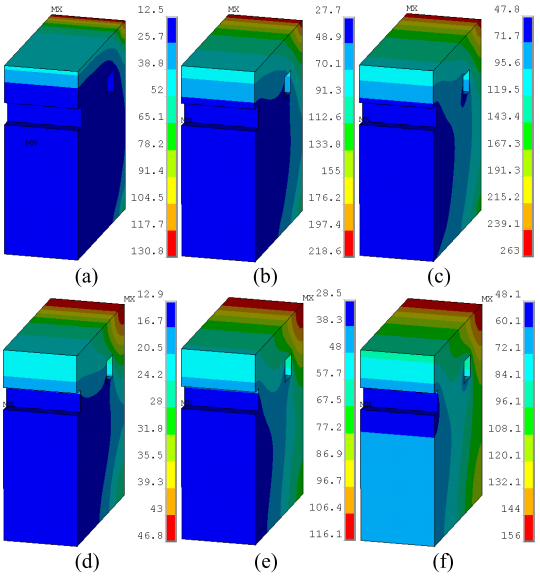

FIGURE 9. Spatial and temporal distribution of temperature near breech in rectangle rail, 20 shots/min, channel cooling, friction coefficient 0.04. (a) t_{1pe}. (b) t_{5pe}. (c) t_{10pe}. (d) t_{1se}. (e) t_{5se}. (f) t_{10se}.

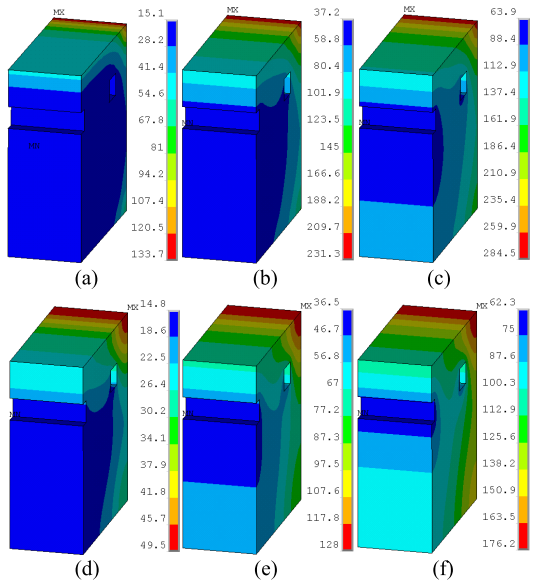

FIGURE 10. Spatial and temporal distribution of temperature near breech in rectangle rail, 20 shots/min, channel cooling, friction coefficient 0.08. (a) t_{1pe}. (b) t_{5pe}. (c) t_{10pe}. (d) t_{1se}. (e) t_{5se}. (f) t_{10se}.

The section area is 14100 mm^2. The detailed parameters are shown in Table 1.

Fig. 2 shows the pulse current waveform used in this article. The simulations are implemented for 10 pulse periods. Fig. 2 just gives the first two pulses. The next 8 pulses are omitted. In Fig. 2, t_{1start} means the first shot start time, t_{1pe} denotes the first pulse end time, t_{1se} represents the first shot end time. The rest symbols could be deduced by analogy. The launch cycle of one shot is from one pulse start time to next pulse start time. It includes a pulse cycle and an interval

FIGURE 11. Spatial and temporal distribution of temperature near breech in rectangle rail, 20 shots/min, channel cooling, friction coefficient 0.12. (a) t_{1pe}. (b) t_{5pe}. (c) t_{10pe}. (d) t_{1se}. (e) t_{5se}. (f) t_{10se}.

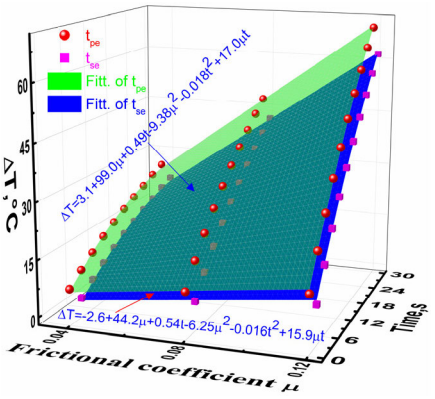

FIGURE 12. Temperature rising caused by friction at t_{pe} and t_{se} in rectangle rails near breech during multi-shot process, by channel cooling, 20 shots/min.

between one pulse and the next one. The current applied is a linear ramped rise current. Its rising, flat and dropping time is 1.5 ms, 6.5 ms and 3.5 ms, respectively. And its maximal value is 3.2 MA. FEM calculations of electromagnetic-thermal coupled field are excuted to compare the thermal features considering friction in three shapes rail under active cooling condition.

III. MATHEMATICAL MODEL

Unsteady temperature field T in the armature and rails is determined by transient heat conduction formula

$$\rho c \frac{\partial T}{\partial t} - \nabla \cdot k \nabla T = \frac{\mathbf{j}^2}{\sigma} + \mathbf{q}_f \tag{1}$$

$$\mathbf{q}_f = \mu P v = \mu (P_0 + P_e) v \tag{2}$$

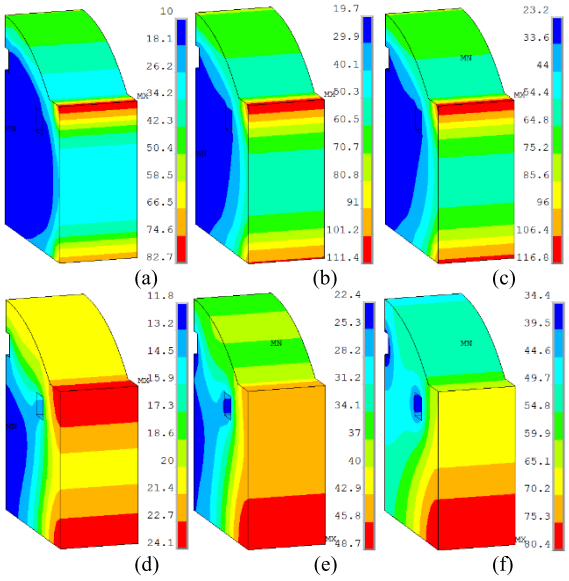

FIGURE 13. Spatial and temporal distribution of temperature near breech in convex rail, 10 shots/min, channel cooling, without friction [23]. (a) t_{1pe}. (b) t_{4pe}. (c) t_{5pe}. (d) t_{1se}. (e) t_{4se}. (f) t_{10se}.

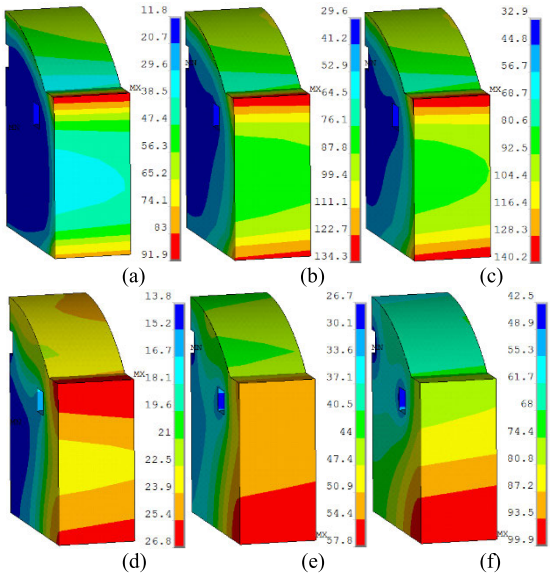

FIGURE 14. Spatial and temporal distribution of temperature near breech in convex rail, 10 shots/min, channel cooling, friction coefficient 0.04. (a) t_{1pe}. (b) t_{5pe}. (c) t_{6pe}. (d) t_{1se}. (e) t_{4se}. (f) t_{10se}.

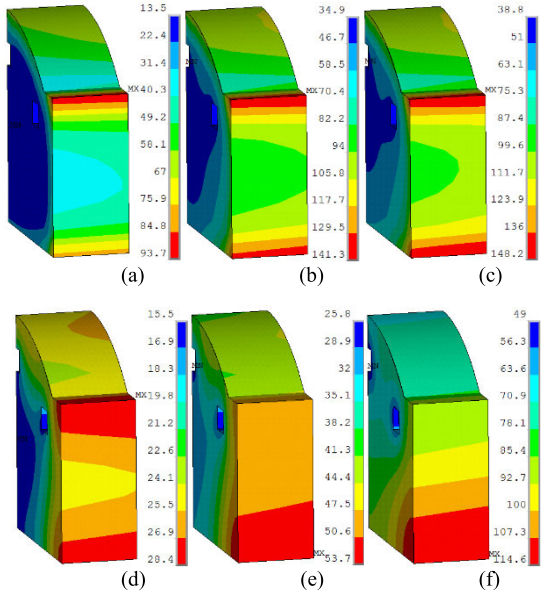

FIGURE 15. Spatial and temporal distribution of temperature near breech in convex rail, 10 shots/min, channel cooling, friction coefficient 0.08. (a) t_{1pe}. (b) t_{5pe}. (c) t_{6pe}. (d) t_{1se}. (e) t_{3se}. (f) t_{10se}.

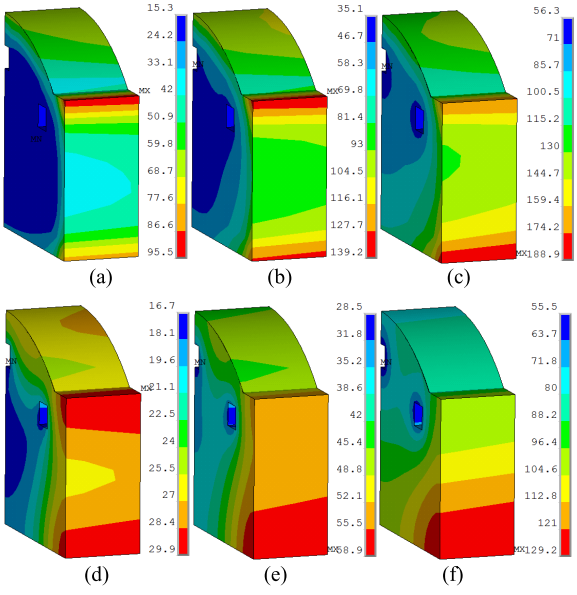

FIGURE 16. Spatial and temporal distribution of temperature near breech in convex rail, 10 shots/min, channel cooling, friction coefficient 0.12. (a) t_{1pe}. (b) t_{4pe}. (c) t_{9pe}. (d) t_{1se}. (e) t_{3se}. (f) t_{10se}.

where c denotes the heat capacity, ρ means the density, k represents the thermal conductivity, σ denotes the electrical conductivity, $\mathbf{j}$ means the current density in conductors, $\mathbf{q}_f$ represents thermal power of friction, μ means friction coefficient between rail and armature, P_0 denotes the preloaded pressure of armature, P_e represents the electromagnetic pressure between armature and rails, v is armature sliding velocity.

The governing formulas of the current density derived from Maxwell formulas as follow

$$\mathbf{j} = -\frac{1}{\mu_0}\nabla^2\mathbf{A} \tag{3}$$

$$\nabla \cdot \mathbf{j} = 0 \tag{4}$$

In the non-conducting area, where current density $\mathbf{j} = 0$, in place of (3), thus

$$\nabla^2\mathbf{A} = 0 \tag{5}$$

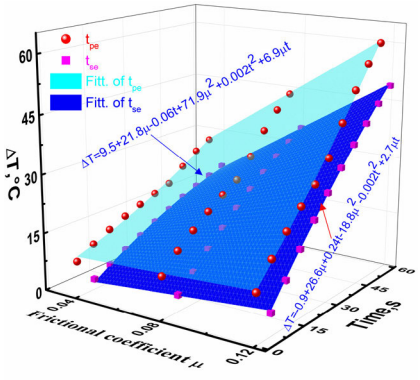

FIGURE 17. Temperature rising caused by friction at t_{pe} and t_{se} in convex rails near breech during multi-shot process, by channel cooling, 10 shots/min.

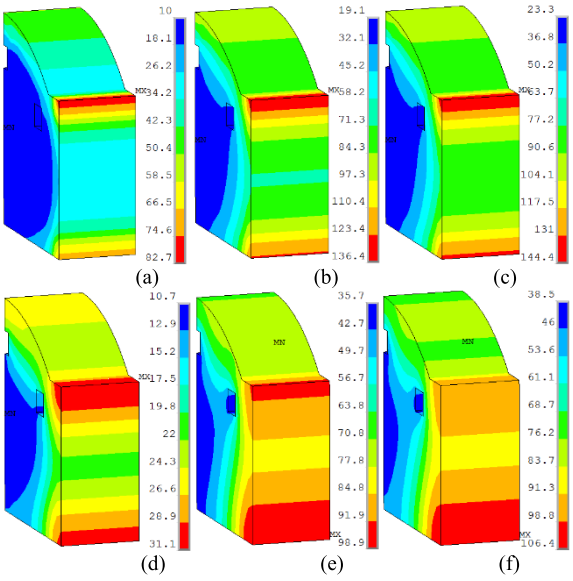

FIGURE 18. Spatial and temporal distribution of temperature near breech in convex rail, 20 shots/min, channel cooling, without friction [23]. (a) t_{1pe}. (b) t_{5pe}. (c) t_{6pe}. (d) t_{1se}. (e) t_{8se}. (f) t_{9se}.

The initial condition of (1) is

$$T_0 = 10^{\circ}C \tag{6}$$

The boundary condition of (1) is

$$-k\frac{\partial T}{\partial n}\bigg|_{\Gamma} = h\left(T - T_f\right)\big|_{\Gamma} \tag{7}$$

where h means heat transfer coefficient, T_f denotes flow temperature.

Formulas (1)–(4) are approximated by the Galerkin weighted residual finite element method in the conductors. The system of linear formulas is solved by Incomplete Cholesky Conjugate Gradient method. The computational domain includes armature, rail, air surrounding the ERL and water flowing in cooling channel. The air region diameter is 0.6 m in computational domain. The domain is covered by nonuniform finite element grid consisting of hexagonal

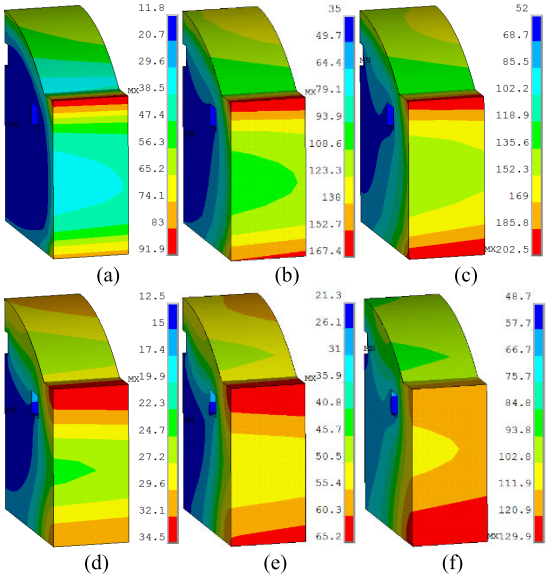

FIGURE 19. Spatial and temporal distribution of temperature near breech in convex rail, 20 shots/min, channel cooling, friction coefficient 0.04. (a) t_{1pe}. (b) t_{6pe}. (c) t_{10pe}. (d) t_{1se}. (e) t_{3se}. (f) t_{9se}.

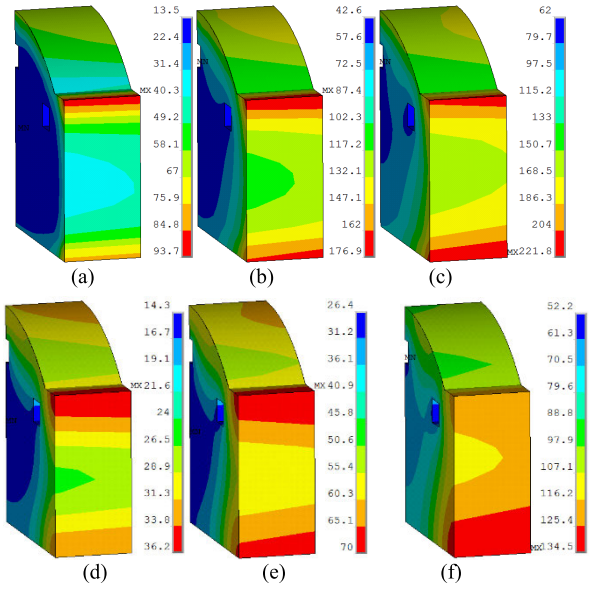

FIGURE 20. Spatial and temporal distribution of temperature near breech in convex rail, 20 shots/min, channel cooling, friction coefficient 0.08. (a) t_{1pe}. (b) t_{6pe}. (c) t_{10pe}. (d) t_{1se}. (e) t_{3se}. (f) t_{8se}.

elements. The element size in cooling water and conductors is 2∼8 mm. The element size in air surrounding ERL is 5∼50 mm. The total element number of computation domain is about 320,000. The time step during current applied is 0.5ms, and the time step during time interval between two sequential pulses is 0.5 s.

The boundary condition of electromagnetic part of the computational domain demands the components of the vector potential vanish at an infinite boundary. At all internal boundaries between the conductors and air, the continuity

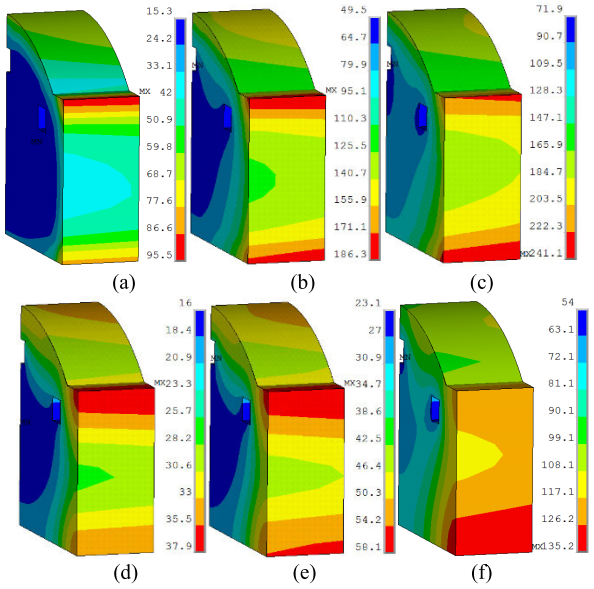

FIGURE 21. Spatial and temporal distribution of temperature near breech in convex rail, 20 shots/min, channel cooling, friction coefficient 0.12. (a) t_{1pe}. (b) t_{6pe}. (c) t_{10pe}. (d) t_{1se}. (e) t_{2se}. (f) t_{7se}.

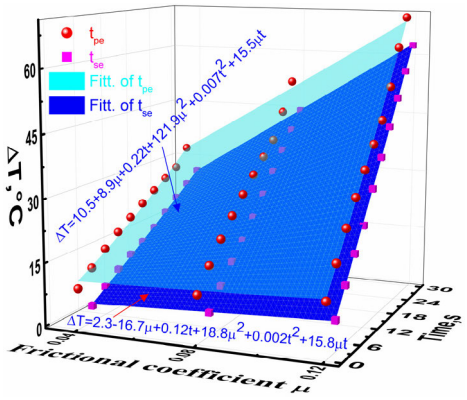

FIGURE 22. Temperature rising caused by friction at t_{pe} and t_{se} in convex rails near breech during multi-shot process, by channel cooling, 20 shots/min.

conditions of the vector-potential components and their derivatives are satisfied.

The boundary conditions of the heat conduction equation (1) specify that heat transfer with the surrounding air is absent in the simulation process, and are simplified to Neumann conditions at all boundaries of the conductors.

IV. THERMAL ANALYSIS IN THREE TYPE RAILS BY CHANNEL COOLING

The friction coefficient between armature and rails in ERL decreases by approximately 50% in the case of high current density (> 10^{10} A/m^2), and is not more than 0.12[24]. Therefore, the sliding friction coefficients are taken as 0, 0.04, 0.08, and 0.12 in this paper. In this section, thermal characteristics in ERL with three shapes rail under active cooling condition with four friction coefficients are analyzed.

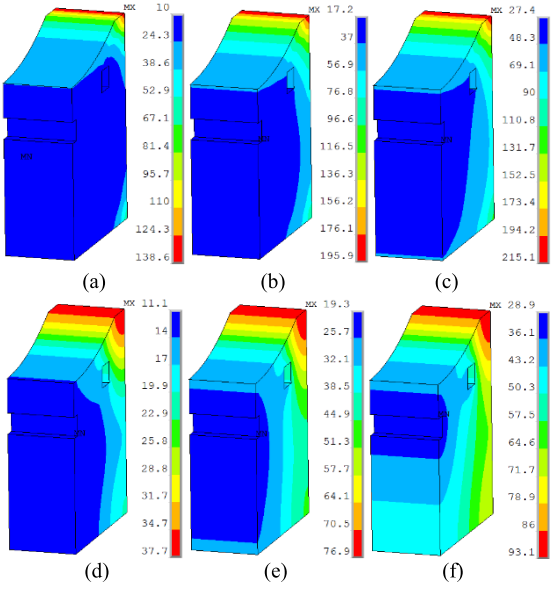

FIGURE 23. Spatial and temporal distribution of temperature near breech in concave rail, 10 shots/min, channel cooling, without friction [23]. (a) t_{1pe}. (b) t_{5pe}. (c) t_{10pe}. (d) t_{1se}. (e) t_{5se}. (f) t_{10se}.

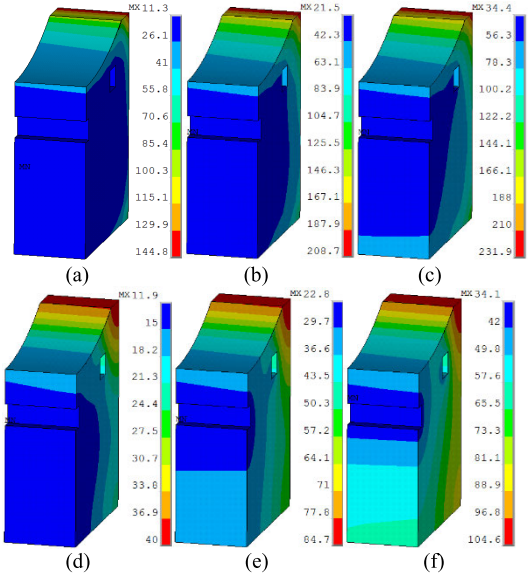

FIGURE 24. Spatial and temporal distribution of temperature near breech in concave rail, 10 shots/min, channel cooling, friction coefficient 0.04. (a) t_{1pe}. (b) t_{5pe}. (c) t_{10pe}. (d) t_{1se}. (e) t_{5se}. (f) t_{10se}.

In general, there are two active cooling approaches for rails in ERL: surface cooling and channel cooling. When using channel cooling method, there is continuous flowing water in cooling channels of rails. Heat transfer coefficient of cooling water in channels h_c was taken as 10000 W/(m^2.K) in this paper. Calculations were done for three shapes rail with channel cooling at two launch rates: 10 shots/min, and 20 shots/min, respectively.

The temperature in breech measured by experiments is the highest in whole rail [17]. At pulse end moment, Joule heat

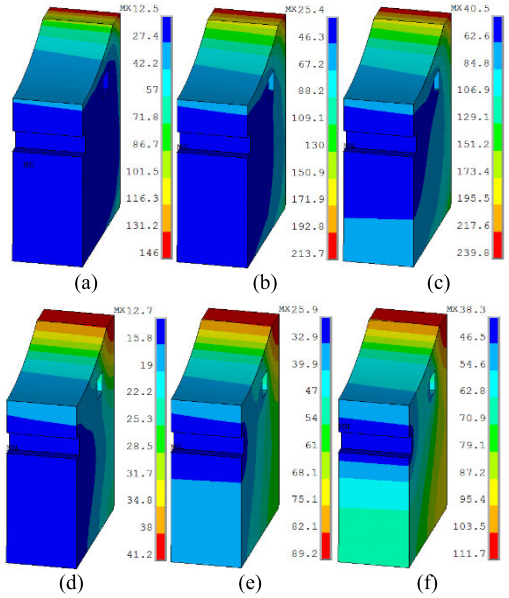

FIGURE 25. Spatial and temporal distribution of temperature near breech in concave rail, 10 shots/min, channel cooling, friction coefficient 0.08. (a) t_{1pe}. (b) t_{5pe}. (c) t_{10pe}. (d) t_{1se}. (e) t_{5se}. (f) t_{10se}.

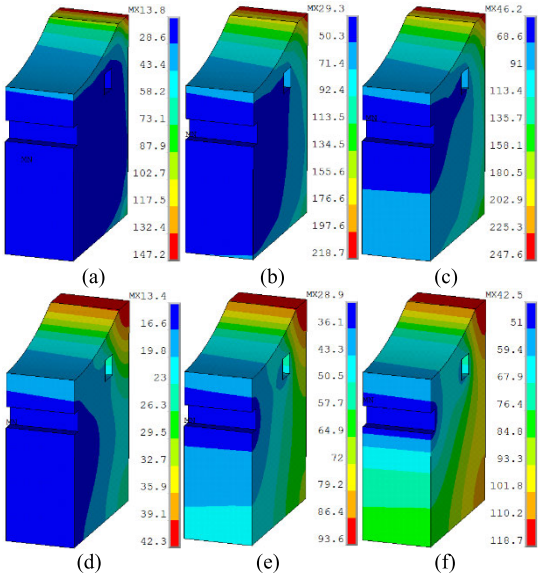

FIGURE 26. Spatial and temporal distribution of temperature near breech in concave rail, 10 shots/min, channel cooling, friction coefficient 0.12. (a) t_{1pe}. (b) t_{5pe}. (c) t_{10pe}. (d) t_{1se}. (e) t_{5se}. (f) t_{10se}.

accumulation reaches its maximum during one shot cycle. Compared with Joule heat, friction heat has less effect on the rail temperature, so rail temperature at pulse end time is the highest during one shot period. Each shot end time is also the start moment of the next one. Temperature nephograms of section near the breech which can intuitively reflect the peak temperature distribution in rails are shown in next two sections.

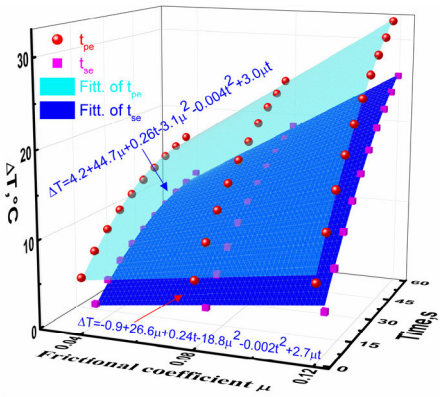

FIGURE 27. Temperature rising caused by friction at t_{pe} and t_{se} in concave rails near breech during multi-shot process, by channel cooling, 10 shots/min.

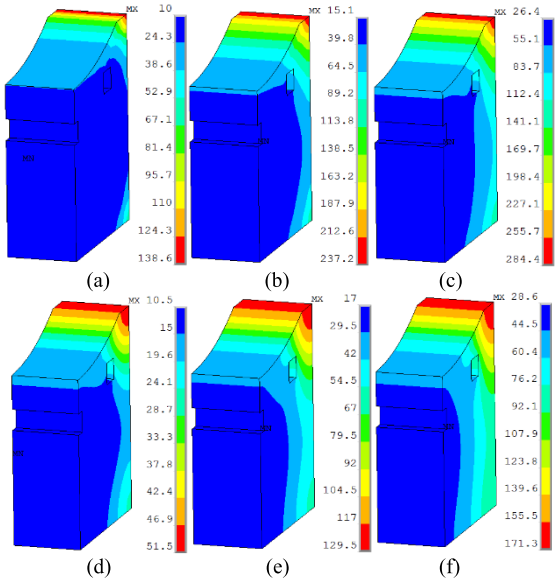

FIGURE 28. Spatial and temporal distribution of temperature near breech in concave rail, 20 shots/min, channel cooling, without friction [23]. (a) t_{1pe}. (b) t_{5pe}. (c) t_{10pe}. (d) t_{1se}. (e) t_{5se}. (f) t_{10se}.

A. SPATIAL AND TEMPORAL DISTRIBUTION CHARACTERISTICS OF RAILS TEMPERATURE IN ERL WITH RECTANGLE RAILS

Spatial and temporal distribution of temperature near breech in rectangle rail by channel cooling at 10 shots/min with friction coefficient 0, 0.04, 0.08, and 0.12 are depicted in Figs. 3–6, respectively. The scale in the nephogram has the units of °C. It is the same in the latter nephograms.

As observed in Figs. 3–6, during 10 shots time, since heat generated by current and friction gradually conducted from rail surface to interior, the temperature in rail interior rises by degrees, but maximal temperature in rails always concentrates in the rail interior edge. With the escalating friction coefficient, the peak temperature in rectangle rails increases at the same time. At pulse end time, the peak

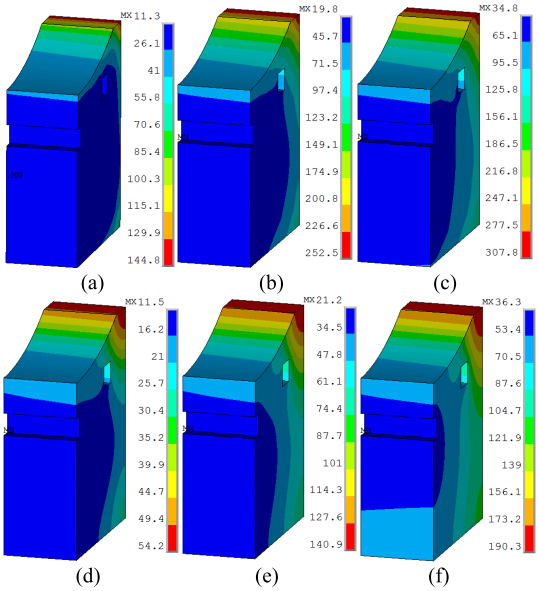

FIGURE 29. Spatial and temporal distribution of temperature near breech in concave rail, 20 shots/min, channel cooling, friction coefficient 0.04. (a) t_{1pe}. (b) t_{5pe}. (c) t_{10pe}. (d) t_{1se}. (e) t_{5se}. (f) t_{10se}.

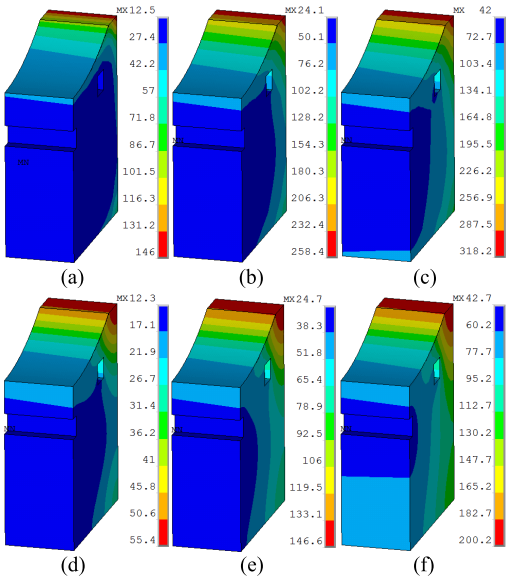

FIGURE 30. Spatial and temporal distribution of temperature near breech in concave rail, 20 shots/min, channel cooling, friction coefficient 0.08. (a) t_{1pe}. (b) t_{5pe}. (c) t_{10pe}. (d) t_{1se}. (e) t_{5se}. (f) t_{10se}.

temperature region is always concentrated in the rail interior edge, regardless of the friction coefficient. With the increase of friction coefficient, peak temperature at t_{se} in rectangle rails will transfer from interior edge to exterior edge in the region near exterior edge after several shots. The higher the friction coefficient, the earlier the transition time occurs.

Temperature rising induced by friction heat at t_{pe} and t_{se} near breech in rectangle rails, at launch rate 10 shots/min, by channel cooling versus friction coefficient and time is illustrated in Fig. 7.

TABLE 2. Temperature rising ΔT comparison in rectangle rails, channel cooling.

μ / time	0.04	0.08	0.12	
t_{1pe}	7.8 °C	10.7 °C	13.7 °C	10 shots/min
t_{10pe}	21.1 °C	39.4 °C	53.5 °C	
t_{1se}	2.6 °C	5.1 °C	7.5 °C	
t_{10se}	16.1 °C	37.3 °C	48.2 °C	
t_{1pe}	7.8 °C	10.7 °C	13.7 °C	20 shots/min
t_{10pe}	26.5 °C	48 °C	69.4 °C	
t_{1se}	3.2 °C	5.9 °C	8.7 °C	
t_{10se}	21.0 °C	41.2 °C	61.3 °C	

As seen in Fig. 7, temperature rising ΔT caused by friction in rectangle rails at t_{pe} is higher than that at t_{se}, at the same friction coefficient μ, by channel cooling, at repetition rate 10 shots/min.

ΔT at t_{pe}, μ, and t can be fitted into equation as follow

$$\Delta T = 6.7 + 31.5\mu + 0.43t + 318.8\mu^2 - 0.002t^2 + 7.5\mu t \quad (8)$$

ΔT at t_{se}, μ, and t meet the following formula

$$\Delta T = 2.2 - 0.7\mu - 0.12t + 43.8\mu^2 - 4.7\times 10^{-4}t^2 + 8.1\mu t \quad (9)$$

Both of these formulas are Poly 2D equation.

Figs. 8–11 demonstrate spatial and temporal distribution features of temperature near breech in rectangle rail by channel cooling at 20 shots/min with friction coefficient 0, 0.04, 0.08, and 0.12, respectively.

As observed in the above four figures, during 10 shots time, by channel cooling, at 20 shots/min, peak temperature at t_{pe} and t_{se} all concentrate in the rail interior edge. Maximal temperature by channel cooling at 20 shots/min is higher than that at 10 shots/min. There is no trend which peak temperature area transfers from interior edge to exterior edge.

As shown in Fig. 12, temperature rising induced by friction in rectangle rails at t_{pe} is also higher than that at t_{se}, under the same condition.

ΔT at t_{pe}, μ, and t can be fitted into formula as follow

$$\Delta T = 3.1 + 99\mu + 0.49t + 9.38\mu^2 - 0.018t^2 + 17.0\mu t \quad (10)$$

ΔT at t_{se}, μ, and t satisfy the following equation

$$\Delta T = 2.6 + 44.2\mu + 0.54t + 6.25\mu^2 - 0.016t^2 + 15.9\mu t \quad (11)$$

Both of these equations are Poly 2D formula.

Table 2 compares ΔT in rectangle rails at first and tenth shot moment by channel cooling in Fig. 7 and Fig. 12. As shown in the Table, with the increase of friction coefficient, at 10 shots/min and 20 shots/min, the temperature rising ΔT induced by friction heat increases obviously, no matter how much friction coefficient is. At the same moment and friction coefficient, the temperature rising ΔT at 20 shots/min is higher than that at 10 shots/min. This is because that shot interval is reduced from 6s to 3s at 20 shot/min.

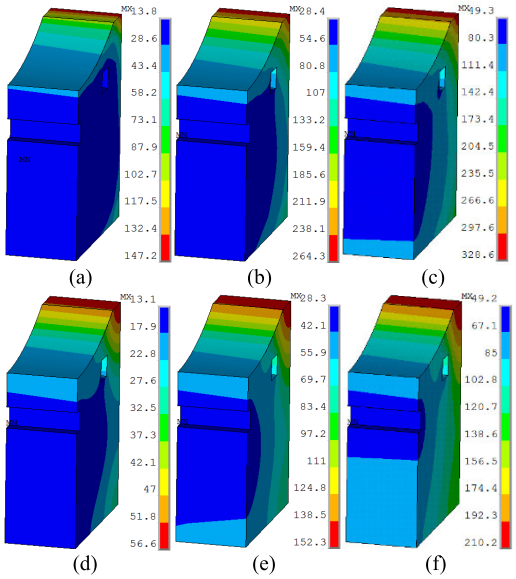

FIGURE 31. Spatial and temporal distribution of temperature near breech in concave rail, 20 shots/min, channel cooling, friction coefficient 0.12. (a) t_{1pe}. (b) t_{5pe}. (c) t_{10pe}. (d) t_{1se}. (e) t_{5se}. (f) t_{10se}.

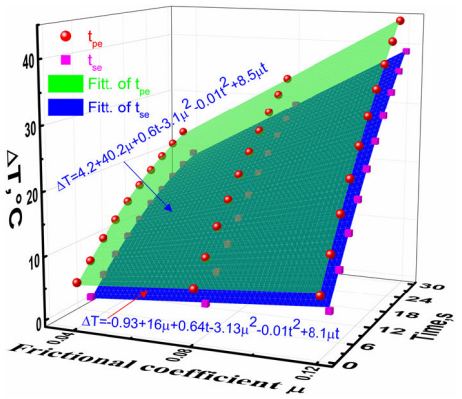

FIGURE 32. Temperature rising at t_{pe} and t_{se} in concave rails near breech during multi-shot process, by channel cooling, 20 shots/min.

B. SPATIAL AND TEMPORAL DISTRIBUTION CHARACTERISTICS OF RAILS TEMPERATURE IN ERL WITH CONVEX RAILS

Spatial and temporal distribution of temperature near breech in convex rail by channel cooling, at 10 shots/min, with friction coefficient 0, 0.04, 0.08, and 0.12 are illustrated in Figs. 13–16, respectively.

As shown in them, during the first several shots, maximal temperature at t_{pe} concentrates in the exterior and interior edges of rail. In the later shots, maximal temperature area at t_{pe} transfers from interior edges to exterior edges of rail. Maximal temperature at t_{se} in convex rails will also transfer from interior edge to exterior edge in the region near exterior edge after several shots. With escalating friction coefficient, peak temperature at the same time increases.

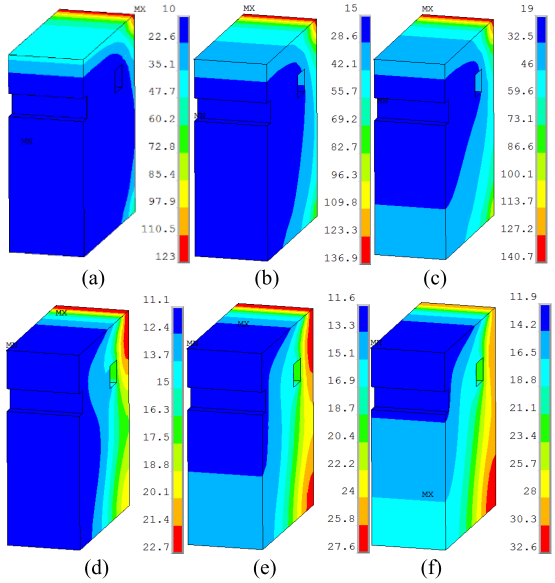

FIGURE 33. Spatial and temporal distribution of temperature near breech in rectangle rail, 10 shots/min, surface/channel cooling, without friction [23]. (a) t_{1pe}. (b) t_{5pe}. (c) t_{10pe}. (d) t_{1se}. (e) t_{2se}. (f) t_{3se}.

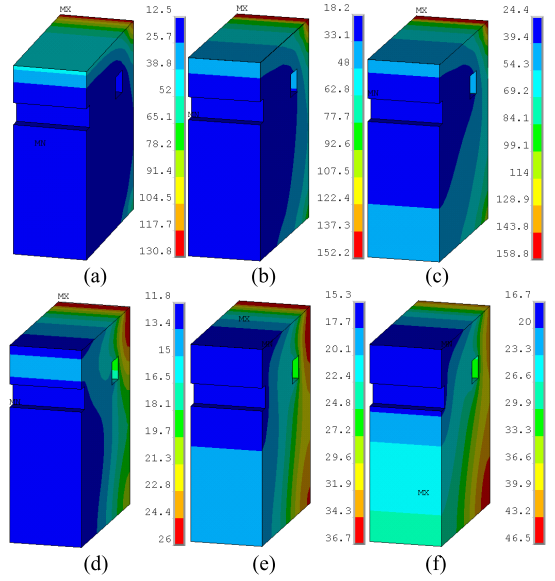

FIGURE 34. Spatial and temporal distribution of temperature near breech in rectangle rail, 10 shots/min, surface/channel cooling, friction coefficient 0.04. (a) t_{1pe}. (b) t_{5pe}. (c) t_{10pe}. (d) t_{1se}. (e) t_{3se}. (f) t_{5se}.

Temperature rising ΔT induced by friction at t_{pe} and t_{se} near breech in convex rails, at 10 shots/min, by channel cooling versus friction coefficient and time is depicted in Fig.17.

As seen in Fig. 17, temperature rising ΔT caused by friction in convex rails at t_{pe} is higher than that at t_{se}, under identical condition.

ΔT at t_{pe}, μ, and t meet the following formula

$$\Delta T = 9.5 + 21.8\mu - 0.06t + 71.9\mu^2 + 0.002t^2 + 6.9\mu t \quad (12)$$

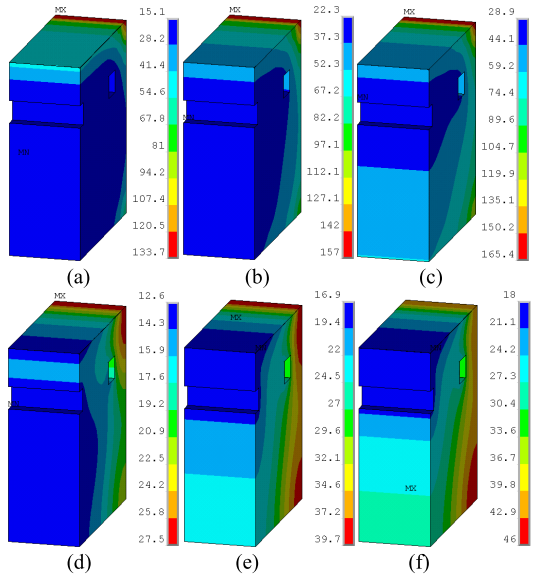

FIGURE 35. Spatial and temporal distribution of temperature near breech in rectangle rail, 10 shots/min, surface/channel cooling, friction coefficient 0.08. (a) t_{1pe}. (b) t_{5pe}. (c) t_{10pe}. (d) t_{1se}. (e) t_{3se}. (f) t_{4se}.

ΔT at t_{se}, μ, and t can be fitted into equation as follow

$$\Delta T = -0.9 + 26.6\mu + 0.24t - 18.8\mu^2 - 0.002t^2 + 2.7\mu t \quad (13)$$

The above two formulas are Poly 2D equation.

As observed in Figs. 18–21, maximal temperature in convex rails by channel cooling at 20 shots/min is higher than that at 10 shots/min. As illustrated in them, by channel cooling, at 20 shots/min, during the first several shots, maximal temperature in convex rails at t_{pe} concentrates in the interior and exterior edges of rail. In the later shots, maximal temperature region at t_{pe} transfers from rail interior edges to rail exterior edges. Peak temperature in convex rails at t_{se} will also transfer from interior edge to exterior edge in the region near exterior edge after several shots.

As shown in Fig. 22, temperature rising induced by friction in convex rails at t_{pe} is higher than that at t_{se}, at the same friction coefficient, by channel cooling, at 20 shots/min.

ΔT at t_{pe}, μ, and t satisfy the following equation

$$\Delta T = 10.5 + 8.9\mu + 0.22t + 121.9\mu^2 + 0.007t^2 + 15.5\mu t \quad (14)$$

ΔT at t_{se}, μ, and t can be fitted into formula as follow

$$\Delta T = 2.3 - 16.7\mu + 0.12t + 18.8\mu^2 + 0.002t^2 + 15.8\mu t \quad (15)$$

The above two equations are Poly 2D formula.

Temperature rising comparison in convex rails by channel cooling at first and tenth shot moment in Table 3 is extracted from Fig. 17 and Fig. 22. As shown in it, with escalating friction coefficient, at 10 shots/min and 20 shots/min, temperature rising caused by friction heat increases clearly, regardless of friction coefficient. At the same condition, the temperature rising in convex rails at 20 shots/min is higher than that at 10 shots/min as well.

TABLE 3. Temperature rising ΔT comparison in convex rails, channel cooling.

time \ μ	0.04	0.08	0.12	
t_{1pe}	9.2 °C	11 °C	12.8 °C	10 shots/min
t_{10pe}	28.6 °C	44.7 °C	60.8 °C	
t_{1se}	2.7 °C	4.3 °C	5.8 °C	
t_{10se}	19.5 °C	34.2 °C	48.8 °C	
t_{1pe}	9.2 °C	11 °C	12.8 °C	20 shots/min
t_{10pe}	33.3 °C	36.9 °C	69.9 °C	
t_{1se}	3.4 °C	5.1 °C	6.8 °C	
t_{10se}	26.1 °C	31.3 °C	62.5 °C	

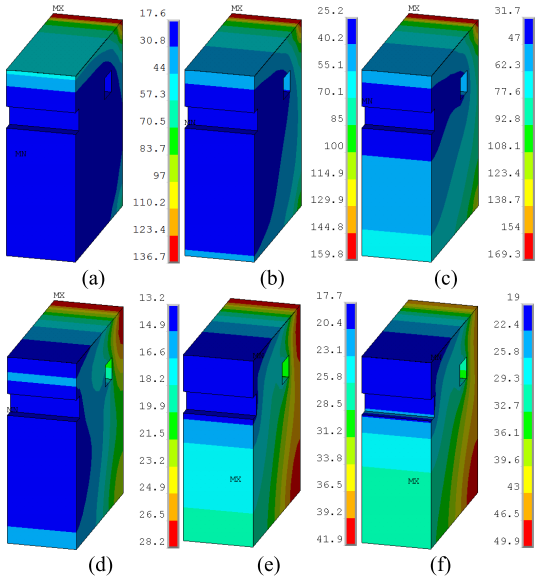

FIGURE 36. Spatial and temporal distribution of temperature near breech in rectangle rail, 10 shots/min, surface/channel cooling, friction coefficient 0.12. (a) t_{1pe}. (b) t_{5pe}. (c) t_{10pe}. (d) t_{1se}. (e) t_{3se}. (f) t_{4se}.

C. SPATIAL AND TEMPORAL DISTRIBUTION CHARACTERISTICS OF RAILS TEMPERATURE IN ERL WITH CONCAVE RAILS

Spatial and temporal distribution of temperature in concave rail by channel cooling, at 10 shots/min, with friction coefficient 0, 0.04, 0.08, and 0.12 are shown in Figs. 23–26, respectively.

As shown in Figs. 23–26, peak temperature always concentrates in the concave rail interior edge, by channel cooling, at 10 shots/min. The trend that maximal temperature region transfer from interior edge to exterior edge is not observed in them. But it could be concluded that maximum temperature will concentrate in the region near concave rail exterior edge after enough shots.

As observed in Fig. 27, temperature rising caused by friction in concave rails at t_{pe} is larger than that at t_{se}, at 10 shots/min, under the same condition.

ΔT at t_{pe}, μ, and t can be fitted into formula as follow

$$\Delta T = 4.2 + 44.7\mu + 0.26t - 3.1\mu^2 - 0.004t^2 + 3.0\mu t \quad (16)$$

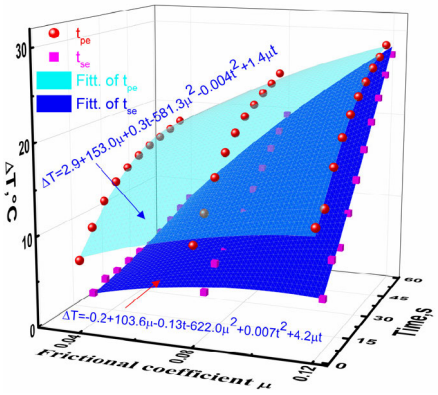

FIGURE 37. Temperature rising caused by friction at t_{pe} and t_{se} in rectangle rails near breech during multi-shot process, by surface/channel cooling, 10 shots/min.

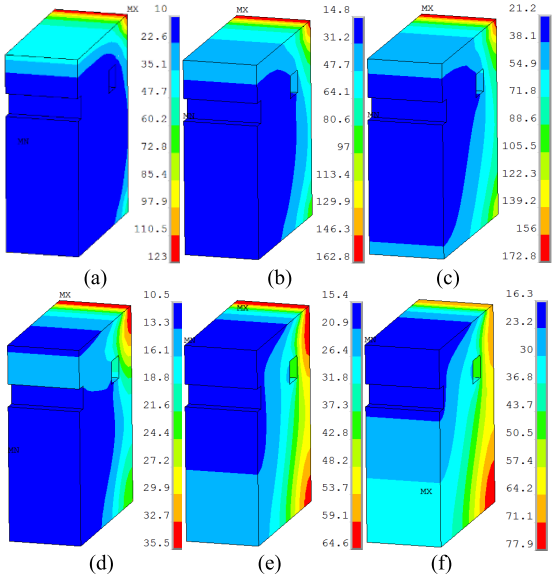

FIGURE 38. Spatial and temporal distribution of temperature near breech in rectangle rail, 20 shots/min, surface/channel cooling, without friction [23]. (a) t_{1pe}. (b) t_{5pe}. (c) t_{10pe}. (d) t_{1se}. (e) t_{6se}. (f) t_{9se}.

ΔT at t_{se}, μ, and t satisfy the following equation

$$\Delta T = -0.9+26.6\mu+0.24t-18.8\mu^2-0.002t^2+2.7\mu t \quad (17)$$

Both of these equations are Poly 2D formula.

Figs. 28–31 demonstrate spatial and temporal distribution of temperature near breech in concave rail by channel cooling, at 20 shots/min, with friction coefficient 0, 0.04, 0.08, and 0.12, respectively. Peak temperature in concave rails by channel cooling at 20 shots/min is higher than that at 10 shots/min. As shown in these figures, maximal temperature concentrates in the concave rail interior edge, by channel cooling, at 20 shots/min, as well.

As observed in Fig. 32, temperature rising induced by friction in concave rails at t_{pe} is higher than that at t_{se}, at the same friction coefficient, by channel cooling, at 20 shots/min.

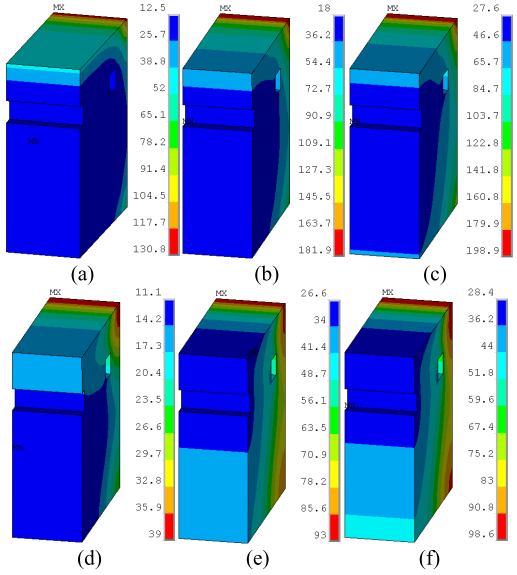

FIGURE 39. Spatial and temporal distribution of temperature near breech in rectangle rail, 20 shots/min, surface/channel cooling, friction coefficient 0.04. (a) t_{1pe}. (b) t_{5pe}. (c) t_{10pe}. (d) t_{1se}. (e) t_{9se}. (f) t_{10se}.

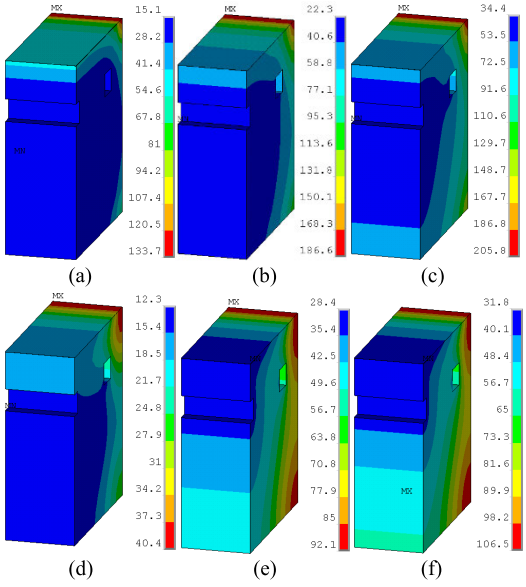

FIGURE 40. Spatial and temporal distribution of temperature near breech in rectangle rail, 20 shots/min, surface/channel cooling, friction coefficient 0.08. (a) t_{1pe}. (b) t_{5pe}. (c) t_{10pe}. (d) t_{1se}. (e) t_{8se}. (f) t_{10se}.

ΔT at t_{pe}, μ, and t can be fitted into equation as follow

$$\Delta T = 4.2+40.2\mu+0.6t-3.1\mu^2-0.01t^2+8.5\mu t \quad (18)$$

ΔT at t_{se}, μ, and t meet the following formula

$$\Delta T = -0.93+16\mu+0.64t-3.13\mu^2-0.01t^2+8.1\mu t \quad (19)$$

Both of these formulas are Poly 2D equation.

Table 4 compares temperature rising in concave rails by channel cooling at first and tenth shot moment in Fig. 27 and Fig. 32. As seen in it, at 10 shots/min and 20 shots/min, with

TABLE 4. Temperature rising ΔT comparison in concave rails, channel cooling.

time \ μ	0.04	0.08	0.12	
t_{1pe}	6.2 °C	7.4 °C	8.7 °C	10 shots/min
t_{10pe}	16.8 °C	24.7 °C	32.5 °C	
t_{1se}	2.3 °C	3.5 °C	4.6 °C	
t_{10se}	11.5 °C	18.6 °C	25.6 °C	
t_{1pe}	6.2 °C	7.4 °C	8.7 °C	20 shots/min
t_{10pe}	23.4 °C	33.8 °C	44.2 °C	
t_{1se}	2.7 °C	3.9 °C	5.2 °C	
t_{10se}	19.0 °C	28.9 °C	38.9 °C	

gradually increasing friction coefficient, the temperature rising induced by friction in concave rails also increases visibly, whatever friction coefficient is. Under the same condition, the temperature rising ΔT at 20 shots/min is also higher than that at 10 shots/min.

Based on the previous results in this Section, the following conclusions could be drawn.

First, by channel cooling, compared with simulation results without friction, peak temperature considering friction in concave rails still is the largest in three types rail, under the same condition. Meanwhile, maximal temperature considering friction in convex rails remain the lowest in three shapes rail, under identical condition. This is because that current distribution in convex rail is more uniform than that in the other two shapes rail [21]. Gouging and ablation usually appear at the high temperature interface between armature and rails. It shows that the possibility that gouging and erosion occurs in convex rails is still the least in three types rail taking friction into account, by channel cooling. By channel cooling, after 10 shots time, the peak temperature in three shapes rail considering friction is tens of degrees higher than that without friction. This indicates that, although Joule heat dominates in rails, friction heat is a nonnegligible part under continuous launching conditions.

Second, there is little difference in temperature rising ΔT caused by friction between rectangle and convex rail, under the same condition. And temperature rising ΔT caused by friction in concave rail is the lowest, under the identical condition. In equation (2), thermal power of friction is related to the preloaded pressure P_0 and electromagnetic pressure P_e. In the case of the same preloaded force in three types rail, the main source of the friction heat difference is electromagnetic force. The electromagnetic force applied on the armature in ERL can be expressed as $F = L'I^2/2$, where L' is the inductance gradient of the rail, I is the current. In [9], inductance gradient in convex rail and rectangle rail is very close, while inductance gradient in concave rail is the smallest. This means that under the same condition, the electromagnetic force in concave rails is minimum in three shapes rail. This could explain the difference among temperature rising in three types rail.

Third, by channel cooling, at two launch rates 10 shots/min and 20 shots/min, temperature rising ΔT caused by friction

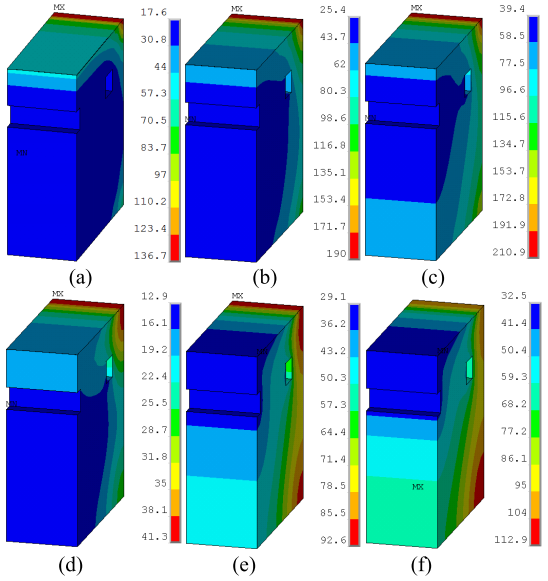

FIGURE 41. Spatial and temporal distribution of temperature near breech in rectangle rail, 20 shots/min, surface/channel cooling, friction coefficient 0.12. (a) t_{1pe}. (b) t_{5pe}. (c) t_{10pe}. (d) t_{1se}. (e) t_{7se}. (f) t_{10se}.

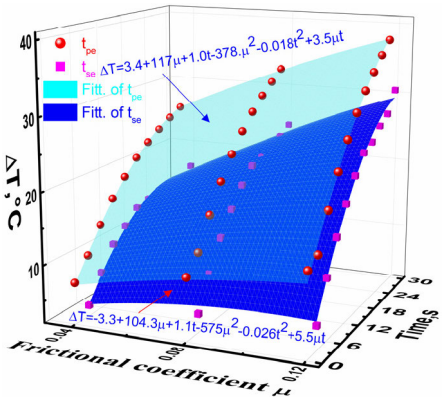

FIGURE 42. Temperature rising caused by friction at t_{pe} and t_{se} in rectangle rails near breech during multi-shot process, by surface/channel cooling, 20 shots/min.

at t_{pe} and t_{se} in three shapes rail, friction coefficient μ, and time t all meet Poly 2D relation.

V. THERMAL ANALYSIS IN THREE TYPE RAILS BY SURFACE/CHANNEL COOLING

While surface/channel cooling technique is implemented, besides channel cooling, cooling water is sprayed on rail interior surface during the interval between one pulse and the next one. Heat transfer coefficient of cooling water flowing in channels h_{c1} is taken as 10000 W/(m^2.K), heat transfer coefficient of water sprayed on interior surface of rails h_{c2} is taken as 20000 W/(m^2.K). Simulations are done for rectangle, convex, and concave rails by surface/channel cooling at two launch rates: 10 shots/min, and 20 shots/min, with friction coefficient 0, 0.04, 0.08, and 0.12, respectively.

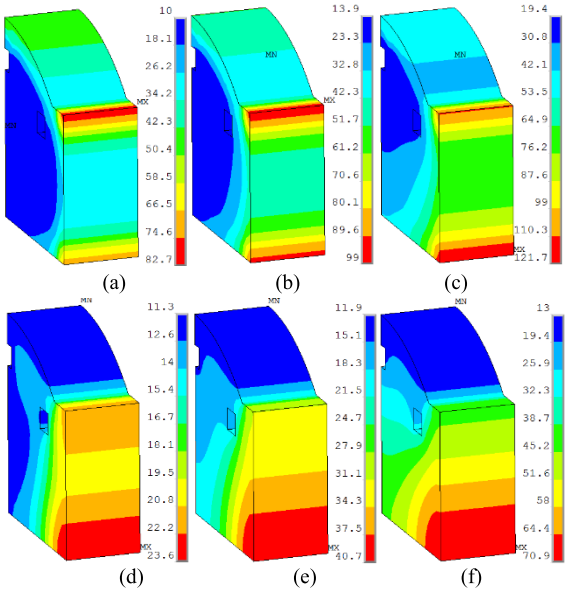

FIGURE 43. Spatial and temporal distribution of temperature near breech in convex rail, 10 shots/min, surface/channel cooling, without friction [23]. (a) t_{1pe}. (b) t_{3pe}. (c) t_{8pe}. (d) t_{1se}. (e) t_{3se}. (f) t_{10se}.

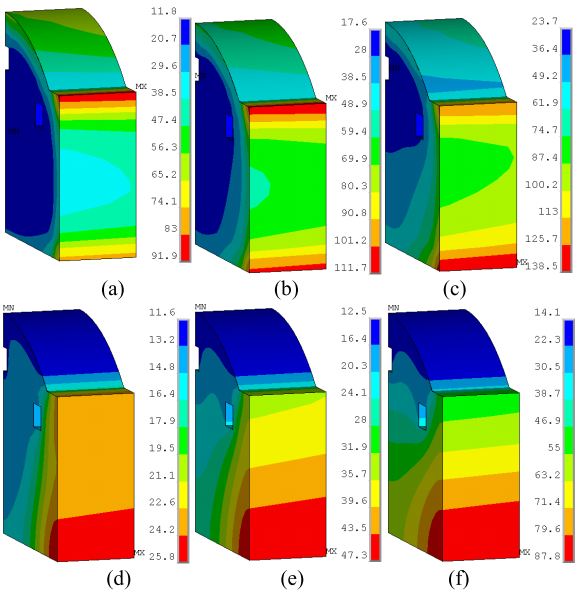

FIGURE 44. Spatial and temporal distribution of temperature near breech in convex rail, 10 shots/min, surface/channel cooling, friction coefficient 0.04. (a) t_{1pe}. (b) t_{3pe}. (c) t_{7pe}. (d) t_{1se}. (e) t_{3se}. (f) t_{10se}.

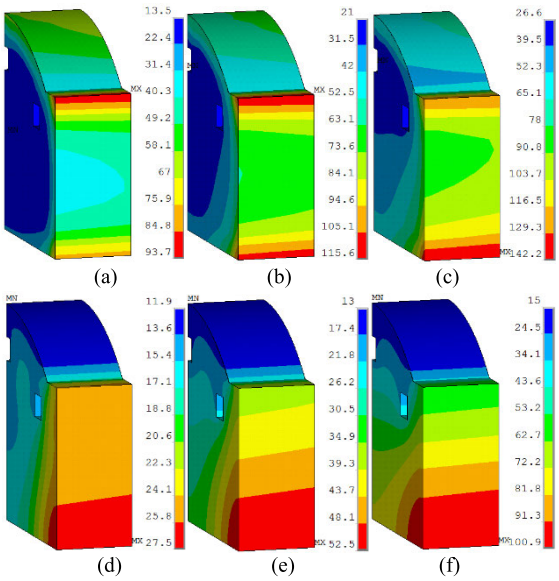

FIGURE 45. Spatial and temporal distribution of temperature near breech in convex rail, 10 shots/min, surface/channel cooling, friction coefficient 0.08. (a) t_{1pe}. (b) t_{3pe}. (c) t_{6pe}. (d) t_{1se}. (e) t_{3se}. (f) t_{10se}.

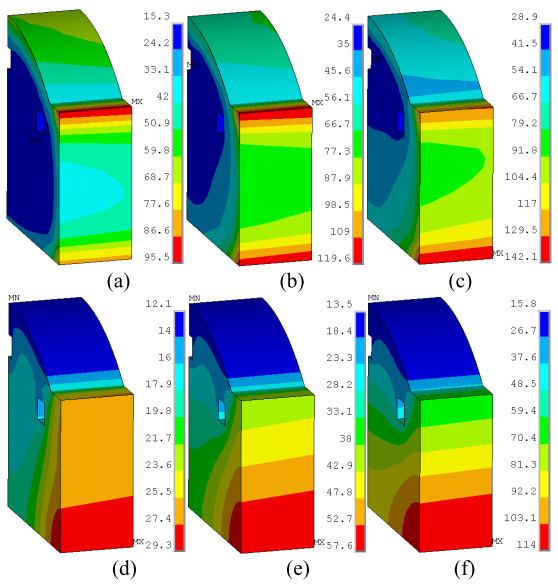

FIGURE 46. Spatial and temporal distribution of temperature near breech in convex rail, 10 shots/min, surface/channel cooling, friction coefficient 0.12. (a) t_{1pe}. (b) t_{3pe}. (c) t_{5pe}. (d) t_{1se}. (e) t_{3se}. (f) t_{10se}.

A. SPATIAL AND TEMPORAL DISTRIBUTION CHARACTERISTICS OF RAILS TEMPERATURE IN ERL WITH RECTANGLE RAILS

Spatial and temporal distribution of temperature in rectangle rail by surface/channel cooling, at 10 shots/min, with friction coefficient 0, 0.04, 0.08, and 0.12 are depicted in Figs. 33–36, respectively.

As observed in them, maximal temperature in rectangle rails by surface/channel cooling at 10 shots/min is lower than that by channel cooling at 10 shots/min. In comparison to channel cooling, low temperature region in rectangle rails by surface/channel cooling cluster in rail interior near cooling channel and rail interior surface. The heat generating near rail interior surface is taken away quickly by cooling water sprayed on rail interior surface. Hence, temperature near interior surface of rail reduce significantly.

As seen in Fig. 37, temperature rising caused by friction heat in rectangle rails at t_{pe} is higher than that at t_{se},

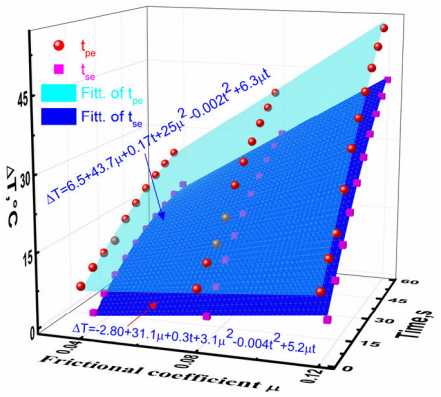

FIGURE 47. Temperature rising caused by friction at t_{pe} and t_{se} in convex rails near breech during multi-shot process, by surface/channel cooling, 10 shots/min.

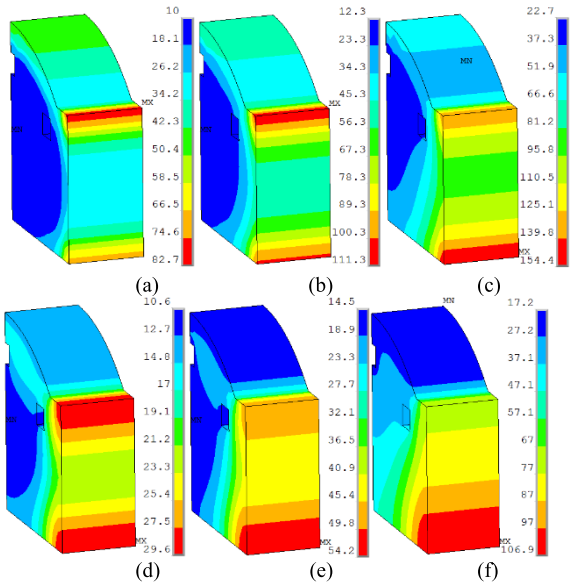

FIGURE 48. Spatial and temporal distribution of temperature near breech in convex rail, 20 shots/min, surface/channel cooling, without friction [23]. (a) t_{1pe}. (b) t_{3pe}. (c) t_{9pe}. (d) t_{1se}. (e) t_{3se}. (f) t_{10se}.

at the same friction coefficient, by surface/channel cooling, at shots/min.

ΔT at t_{pe}, μ, and t can be fitted into formula as follow

$$\Delta T = 2.9+153\mu+0.3t-581.3\mu^2-0.004t^2+1.4\mu t \quad (20)$$

ΔT at t_{se}, μ, and t meet the following equation

$$\Delta T = -0.2+103.6\mu-0.13t-622\mu^2+0.007t^2+4.2\mu t \quad (21)$$

Both of these formulas are Poly 2D equation.

Figs. 38–41 illustrate the spatial and temporal distribution of temperature in rectangle rail by surface/channel cooling at 20 shots/min with friction coefficient 0, 0.04, 0.08, and 0.12, respectively.

As observed in Figs. 38–41, peak temperature in rectangle rails by surface/channel cooling at 20 shots/min is lower than that by channel cooling at the same repetition

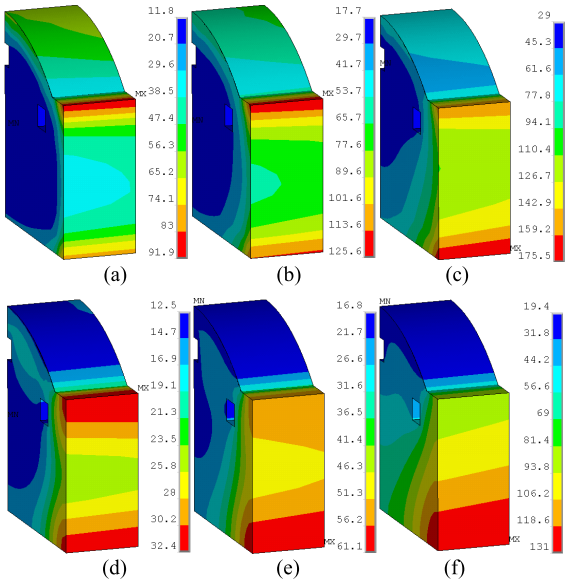

FIGURE 49. Spatial and temporal distribution of temperature near breech in convex rail, 20 shots/min, surface/channel cooling, friction coefficient 0.04. (a) t_{1pe}. (b) t_{3pe}. (c) t_{8pe}. (d) t_{1se}. (e) t_{3se}. (f) t_{10se}.

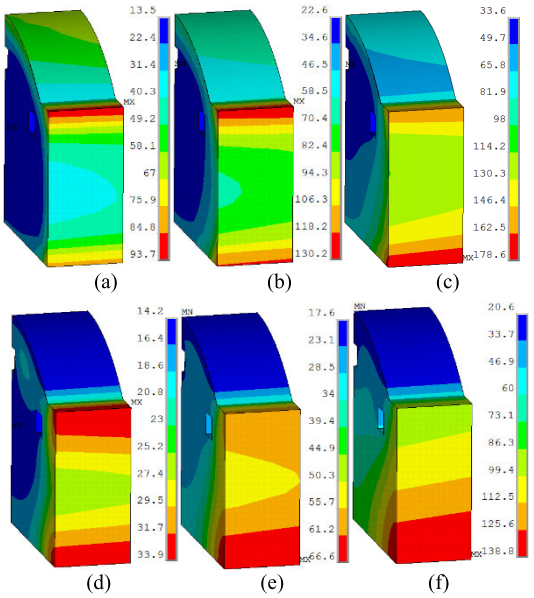

FIGURE 50. Spatial and temporal distribution of temperature near breech in convex rail, 20 shots/min, surface/channel cooling, friction coefficient 0.08. (a) t_{1pe}. (b) t_{3pe}. (c) t_{7pe}. (d) t_{1se}. (e) t_{3se}. (f) t_{9se}.

rate. In comparison to peak temperature in rectangle rails by surface/channel cooling at 10 shots/min, the maximal temperature at 20 shots/min is higher than that in rectangle rails by surface/channel cooling.

As observed in Fig. 42, temperature rising induced by friction in rectangle rails at t_{pe} is higher than that at t_{se}, at the same friction coefficient, by surface/channel cooling, at 20 shots/min. At the same moment and friction coefficient, the temperature rising at 20 shots/min is higher than that at 10 shots/min.

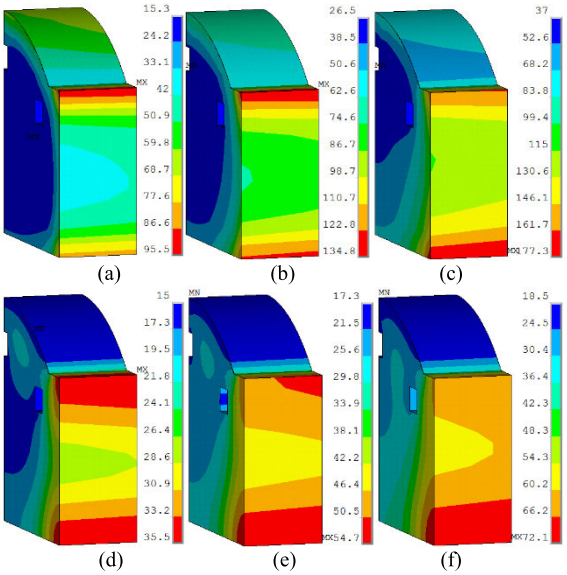

FIGURE 51. Spatial and temporal distribution of temperature near breech in convex rail, 20 shots/min, surface/channel cooling, friction coefficient 0.12. (a) t_{1pe}. (b) t_{3pe}. (c) t_{6pe}. (d) t_{1se}. (e) t_{2se}. (f) t_{3se}.

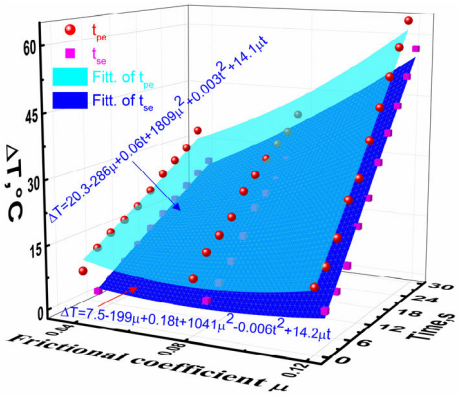

FIGURE 52. Temperature rising caused by friction at t_{pe} and t_{se} in convex rails near breech during multi-shot process, by surface/channel cooling, 20 shots/min.

TABLE 5. Temperature rising ΔT comparison in rectangle rails, surface/channel cooling.

μ / time	0.04	0.08	0.12	
t_{1pe}	7.8 °C	10.7 °C	13.7 °C	10 shots/min
t_{10pe}	18.1 °C	24.7 °C	28.6 °C	
t_{1se}	3.3 °C	4.8 °C	5.5 °C	
t_{10se}	7.7 °C	19.2 °C	27.2 °C	
t_{1pe}	7.8 °C	10.7 °C	13.7 °C	20 shots/min
t_{10pe}	26.1 °C	33 °C	38.1 °C	
t_{1se}	3.5 °C	4.9 °C	5.8 °C	
t_{10se}	16.1 °C	24 °C	30.4 °C	

ΔT at t_{pe}, μ, and t meet the following equation

$$\Delta T = 3.4+117\mu+1.0t-378\mu^2-0.018t^2+3.5\mu t \quad (22)$$

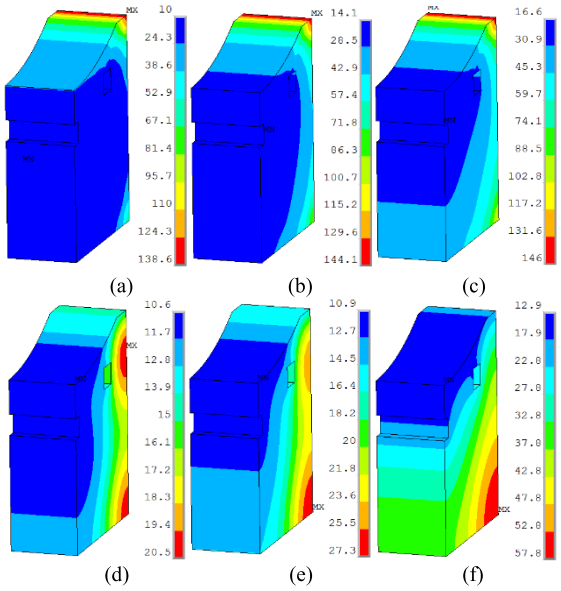

FIGURE 53. Spatial and temporal distribution of temperature near breech in concave rail, 10 shots/min, surface/channel cooling, without friction [23]. (a) t_{1pe}. (b) t_{5pe}. (c) t_{10pe}. (d) t_{1se}. (e) t_{2se}. (f) t_{10se}.

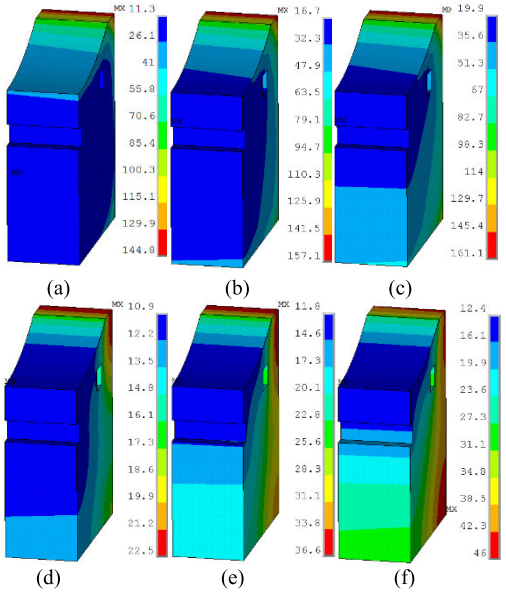

FIGURE 54. Spatial and temporal distribution of temperature near breech in concave rail, 10 shots/min, surface/channel cooling, friction coefficient 0.04. (a) t_{1pe}. (b) t_{5pe}. (c) t_{10pe}. (d) t_{1se}. (e) t_{3se}. (f) t_{5se}.

ΔT at t_{se}, μ, and t can be fitted into formula as follow

$$\Delta T = -3.3+104.3\mu+1.1t-575\mu^2-0.026t^2+5.5\mu t \quad (23)$$

Both of these equations are Poly 2D formula.

Temperature rising comparison in rectangle rails by surface/channel cooling at first and tenth shot moment in Table 5 is excerpted from Fig. 37 and Fig. 42. As shown in it, with escalating friction coefficient, at 10 shots/min and 20 shots/min, temperature rising ΔT induced by friction with surface/channel cooling also increases obviously,

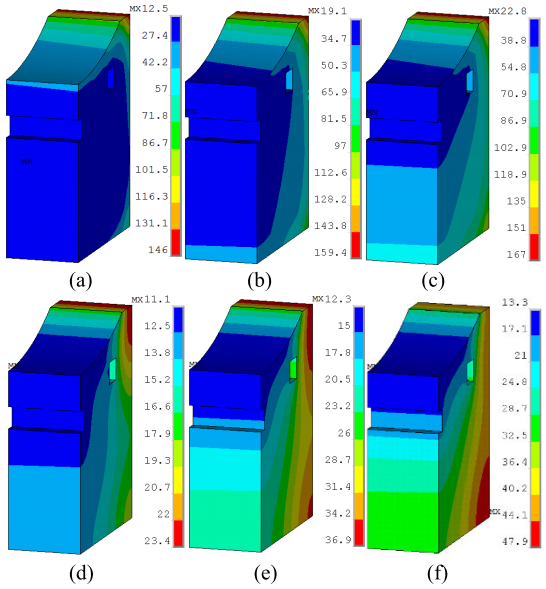

FIGURE 55. Spatial and temporal distribution of temperature near breech in concave rail, 10 shots/min, surface/channel cooling, friction coefficient 0.08. (a) t_{1pe}. (b) t_{5pe}. (c) t_{10pe}. (d) t_{1se}. (e) t_{3se}. (f) t_{5se}.

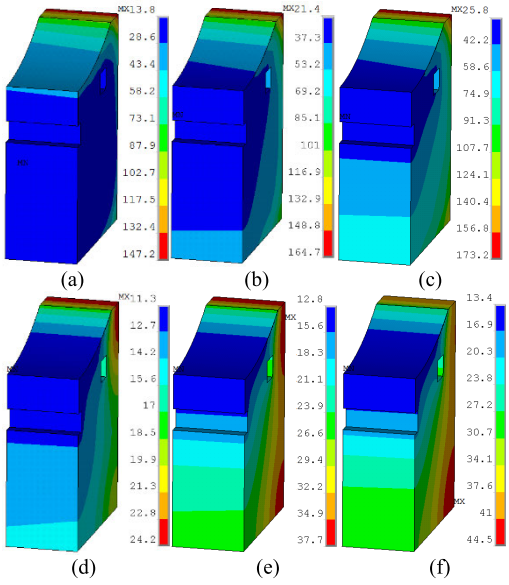

FIGURE 56. Spatial and temporal distribution of temperature near breech in concave rail, 10 shots/min, surface/channel cooling, friction coefficient 0.12. (a) t_{1pe}. (b) t_{5pe}. (c) t_{10pe}. (d) t_{1se}. (e) t_{3se}. (f) t_{4se}.

no matter how much friction coefficient is. Compared with results in Table 2, temperature rising in Table 5 is lower than that by channel cooling, under the same condition. This indicates that surface/channel cooling can more effectively reduce the temperature rising induced by friction. This implies that surface cooling can effectively improve the cooling performance in rectangle rails.

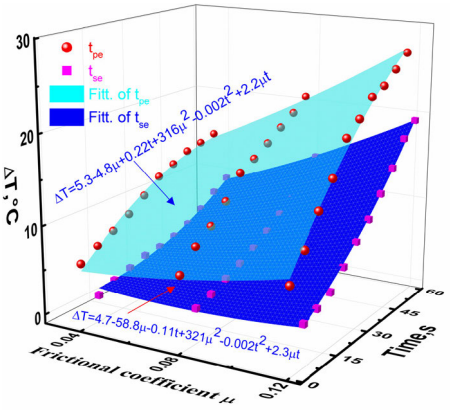

FIGURE 57. Temperature rising caused by friction at t_{pe} and t_{se} in concave rails near breech during multi-shot process, by surface/channel cooling, 10 shots/min.

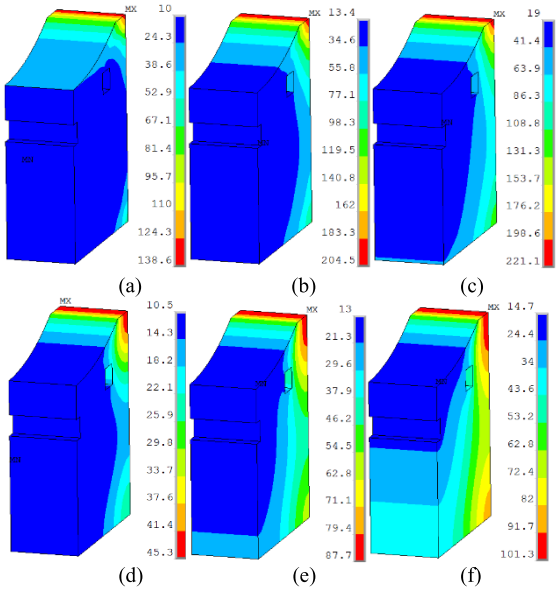

FIGURE 58. Spatial and temporal distribution of temperature near breech in concave rail, 20 shots/min, surface/channel cooling, without friction [23]. (a) °C t_{1pe}. (b) t_{5pe}. (c) t_{10pe}. (d) t_{1se}. (e) t_{5se}. (f) t_{10se}.

B. SPATIAL AND TEMPORAL DISTRIBUTION CHARACTERISTICS OF RAILS TEMPERATURE IN ERL WITH CONVEX RAILS

Spatial and temporal distribution of temperature near breech in convex rail by surface/channel cooling, at 10 shots/min, with friction coefficient 0, 0.04, 0.08, and 0.12 are shown in Figs. 43–46, respectively.

As shown in Figs. 43–46, peak temperature in convex rails by surface/channel cooling at 10 shots/min is lower than that by channel cooling at 10 shots/min. Compared to channel cooling, at 10 shots/min, peak temperature in convex rails by surface/channel cooling is lower with the identical condition. In 10 shots time, the maximal temperature at the first two t_{pe} concentrate in the interior edge of convex rail, regardless of

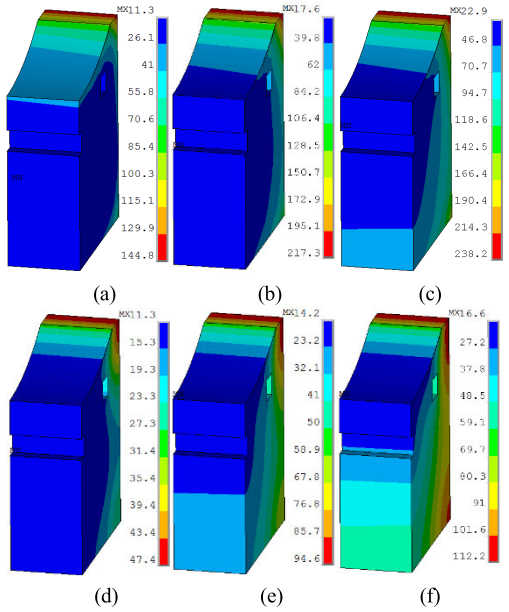

FIGURE 59. Spatial and temporal distribution of temperature near breech in concave rail, 20 shots/min, surface/channel cooling, friction coefficient 0.04. (a) t_{1pe}. (b) t_{5pe}. (c) t_{10pe}. (d) t_{1se}. (e) t_{5se}. (f) t_{10se}.

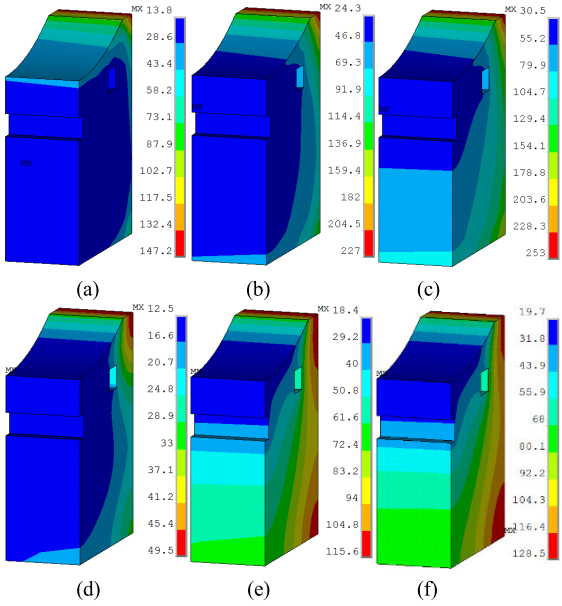

FIGURE 61. Spatial and temporal distribution of temperature near breech in concave rail, 20 shots/min, surface/channel cooling, friction coefficient 0.12. (a) t_{1pe}. (b) t_{5pe}. (c) t_{10pe}. (d) t_{1se}. (e) t_{8se}. (f) t_{10se}.

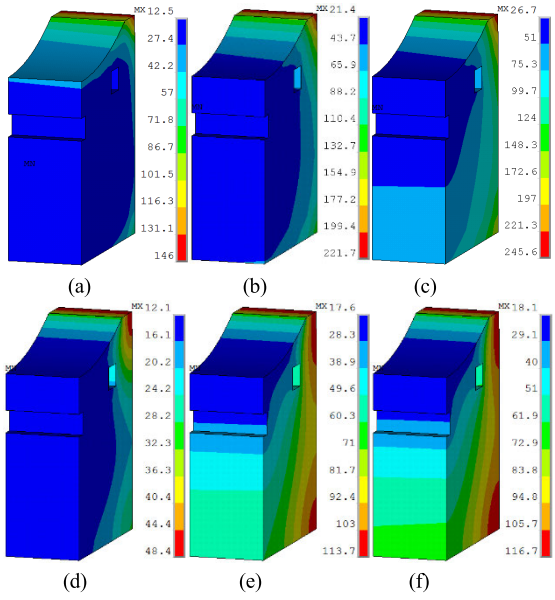

FIGURE 60. Spatial and temporal distribution of temperature near breech in concave rail, 20 shots/min, surface/channel cooling, friction coefficient 0.08. (a) t_{1pe}. (b) t_{5pe}. (c) t_{10pe}. (d) t_{1se}. (e) t_{9se}. (f) t_{10se}.

the friction coefficient. The maximal temperature at middle several t_{pe} cluster in the exterior and interior edges of convex rail. The maximal temperature at the later t_{pe} concentrate in the exterior edge of convex rail. The larger the friction coefficient, the earlier the transition time occurs.

Despite of different friction coefficient, in 10 shots time, by surface/channel cooling, at 10 shots/min, peak temperature at t_{se} all cluster in the convex rail exterior edge. This is because that the sprayed water removes the majority heat near interior edge of rail.

As seen in Fig. 47, temperature rising caused by friction in convex rails at t_{pe} is higher than that at t_{se}, at the same friction coefficient, by surface/channel cooling, at launch rate 10 shots/min. With the increase of friction coefficient, the temperature rising induced by friction in convex rails also increases visibly, no matter how much friction coefficient is.

ΔT at t_{pe}, μ, and t meet the following formula

$$\Delta T = 6.5+43.7\mu+0.17t+25\mu^2 - 0.002t^2+6.3\mu t \quad (24)$$

ΔT at t_{se}, μ, and t can be fitted into equation as follow

$$\Delta T = -2.8+31.1\mu+0.3t+3.1\mu^2 - 0.004t^2+5.2\mu t \quad (25)$$

The above two formulas are Poly 2D equation.

Spatial and temporal distribution of temperature near breech in convex rail by surface/channel cooling at 20 shots/min with friction coefficient 0, 0.04, 0.08, and 0.12 are illustrated in Figs. 48–51, respectively.

As observed in Figs. 48–51, peak temperature in convex rails by surface/channel cooling at 20 shots/min is higher than that by surface/channel cooling at 10 shots/min. Compared with 10 shots/min, peak temperature in convex rails at 20 shots/min by surface/channel cooling is larger.

In 10 shots time, the maximal temperature at the first two t_{pe} concentrate in the convex rail interior edge, regardless of the friction coefficient. This implies that heat generating near the interior edge has not conducted into rail much in first two cycles at 20 shot/min. The maximal temperature at middle several t_{pe} cluster in the exterior and interior edges of convex rail. The maximal temperature at the later t_{pe} concentrate

TABLE 6. Temperature rising ΔT comparison in convex rails, surface/channel cooling.

μ / time	0.04	0.08	0.12	
t_{1pe}	9.2 °C	11 °C	12.8 °C	10 shots/min
t_{10pe}	25.3 °C	40 °C	54.6 °C	
t_{1se}	2.2 °C	3.9 °C	5.7 °C	
t_{10se}	16.9 °C	30.0 °C	43.1 °C	
t_{1pe}	9.2 °C	11 °C	12.8 °C	20 shots/min
t_{10pe}	33.1 °C	35.3 °C	63.8 °C	
t_{1se}	2.8 °C	4.3 °C	5.9 °C	
t_{10se}	24.1 °C	33.9 °C	56.6 °C	

in the exterior edge of convex rail. The higher the friction coefficient, the earlier the transition time.

Maximal temperature at first two t_{se} cluster in the exterior and interior edges of convex rail. As the result of reduced spraying time, heat concentrating near the interior edge is not taken away as quickly as at 10 shots/min. The peak temperature after t_{3se} concentrates in rail exterior edge by surface/channel cooling at 20 shots/min.

As shown in Fig. 52, temperature rising induced by friction in convex rails at t_{pe} is higher than that at t_{se}, at the same friction coefficient, by surface/channel cooling, at 20 shots/min. At the same moment and friction coefficient, the temperature rising at 20 shots/min is higher than that at 10 shots/min. With the increase of friction coefficient, the temperature rising caused by friction also escalate clearly, regardless of friction coefficient.

ΔT at t_{pe}, μ, and t can be fitted into equation as follow

$$\Delta T = 20.3-286\mu+0.06t+1809\mu^2+0.003t^2+14.1\mu t \quad (26)$$

ΔT at t_{se}, μ, and t meet the following formula

$$\Delta T = 7.5+199\mu+0.18t+1041\mu^2-0.006t^2+14.2\mu t \quad (27)$$

The above two equations are Poly 2D formula.

Temperature rising comparison in convex rails by surface/channel cooling at first and tenth shot moment in Table 6 is excerpted from Fig. 47 and Fig. 52. As observed in it, with escalating friction coefficient, at 10 shots/min and 20 shots/min, the temperature rising caused by friction heat also increases distinctly, regardless of friction coefficient. Compared with data in Table 3, temperature rising in Table 6 is lower than that by channel cooling, under the identical condition. This implies that surface cooling can effectively increase the cooling property in convex rails.

C. SPATIAL AND TEMPORAL DISTRIBUTION CHARACTERISTICS OF RAILS TEMPERATURE IN ERL WITH CONCAVE RAILS

By surface/channel cooling, at 10 shots/min, spatial and temporal distribution of temperature near breech in concave rail with friction coefficient 0, 0.04, 0.08, and 0.12 are depicted in Figs. 53–56, respectively.

As observed in Figs. 53–56, by surface/channel cooling, at 10 shots/min, maximal temperature at t_{pe} always concentrates

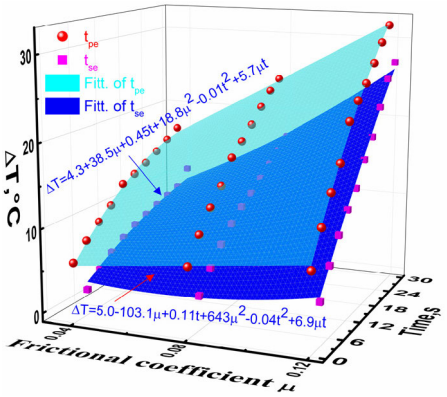

FIGURE 62. Temperature rising caused by friction at t_{pe} and t_{se} in concave rails near breech during multi-shot process, by surface/channel cooling, 20 shots/min.

in the interior edge of concave rails, regardless of friction coefficient. By surface/channel cooling, 10 shots/min, peak temperature at t_{se} will concentrate in the concave rail exterior edge after enough shots.

As shown in Fig. 57, temperature rising caused by friction in concave rails at t_{pe} is higher than that at t_{se}, at the same friction coefficient, by surface/channel cooling, at 10 shots/min.

ΔT at t_{pe}, μ, and t can be fitted into formula as follow

$$\Delta T = 5.3-4.8\mu+0.22t+316\mu^2-0.002t^2+2.2\mu t \quad (28)$$

ΔT at t_{se}, μ, and t satisfy the following equation

$$\Delta T = 4.7–58.8\mu-0.11t+321\mu^2-0.002t^2+2.3\mu t \quad (29)$$

Both of these equations are Poly 2D formula.

Spatial and temporal distribution of temperature near breech in concave rail by surface/channel cooling at 20 shots/min with friction coefficient 0, 0.04, 0.08, and 0.12 are illustrated in Figs. 58–61, respectively.

As shown in Figs. 58–61, by surface/channel cooling, at 20 shots/min, despite of different friction coefficient, peak temperature at t_{pe} always concentrates in concave rail interior edge. By surface/channel cooling, at 20 shots/min, peak temperature at t_{se} will also concentrate in the rail exterior edge after enough shots. The transforming time at this repetition rate is later than that at 10 shots/min.

As observed in Fig. 62, temperature rising ΔT induced by friction in concave rails at t_{pe} is higher than that at t_{se}, at the same friction coefficient μ, by surface/channel cooling, at 20 shots/min. At the same moment and friction coefficient, the temperature rising in concave rails at 20 shots/min is higher than that at 10 shots/min. With incrementally increasing friction coefficient, the temperature rising caused by friction also increases clearly, regardless of friction coefficient. Temperature rising by surface/channel cooling in Fig. 62 is lower than results in Fig. 32 by channel cooling, under the identical condition. This indicates that surface cooling can effectively reduce the temperature rising induced by friction.

TABLE 7. Temperature rising ΔT comparison in concave rails, surface/channel cooling.

μ / time	0.04	0.08	0.12	
t_{1pe}	6.2 °C	7.4 °C	8.7 °C	10 shots/min
t_{10pe}	15.1 °C	21 °C	27.2 °C	
t_{1se}	2.0 °C	2.9 °C	3.7 °C	
t_{10se}	8.9 °C	13.2 °C	19.0 °C	
t_{1pe}	6.2 °C	7.4 °C	8.7 °C	20 shots/min
t_{10pe}	17.1 °C	24.5 °C	31.9 °C	
t_{1se}	2.1 °C	3.1 °C	4.2 °C	
t_{10se}	10.9 °C	15.4 °C	27.2 °C	

ΔT at t_{pe}, μ, and t satisfy the following equation

$$\Delta T = 4.3+38.5\mu+0.45t+18.8\mu^2-0.01t^2+5.7\mu t \quad (30)$$

ΔT at t_{se}, μ, and t can be fitted into formula as follow

$$\Delta T = 5.0-103.1\mu+0.11t+643\mu^2-0.04t^2+6.9\mu t \quad (31)$$

Both of these formulas are Poly 2D equation.

Table 7 compares temperature rising in concave rails by surface/channel cooling at first and tenth shot moment in Fig. 57 and Fig. 62. As shown in it, with gradually increasing friction coefficient, at 10 shots/min and 20 shots/min, the temperature rising induced by friction heat in concave rails also escalates visibly, no matter how much friction coefficient is. Compared with data in Table 4, temperature rising in Table 7 is also lower than that by channel cooling, under the same condition.

On the basis of foregoing analysis in Section V, the study of this section obtained conclusions as follows.

Firstly, compared with simulation results without friction, by surface/channel cooling, maximal temperature considering friction in concave rails still is the largest in three types rail, under the identical condition. Meanwhile, peak temperature considering friction in convex rails remain the lowest in three shapes rail, under same condition. By surface/channel cooling, after 10 shots, the maximal temperature in three types rail considering friction is several degrees to dozens of degrees higher than that without friction. This implies that, by surface/channel cooling, although Joule heat is the main part of heat in rails, friction heat is not a neglected part during continuous launching process.

Secondly, by surface/channel cooling, temperature rising ΔT induced by friction in concave rail remains the lowest in three shapes rail, under the identical condition.

Thirdly, by surface/channel cooling, at two launch rates 10 shots/min and 20 shots/min, temperature rising ΔT induced by friction at t_{pe} and t_{se} in three types rail, friction coefficient μ, and time t satisfy Poly 2D relation, as well.

VI. CONCLUSION

In this article, thermal features in which friction heat is taken into account are researched for the section of rectangle, convex, and concave rails with active cooling condition.

The spatial and temporal distribution characteristics of peak temperature in three types rail considering friction heat under active cooling condition are comparatively studied. Compared with the results without friction, by channel and surface/channel cooling approaches, at 10 shots/min and 20 shots/min, with the same friction coefficient and time, the peak temperature in concave rail is still maximum and the maximal temperature in convex rail remain the minimum when considering friction.

As the launch times increases, the temperature rising caused by friction augments correspondingly. Joule heat still dominates in rails when friction is considered, but friction heat is a non-negligible component in multi-shot launch process.

With channel and surface/channel cooling methods, temperature rising ΔT caused by friction in concave rail remains the lowest in three shapes rail, under the identical condition.

By channel cooling and surface/channel cooling, at 10 shots/min and 20 shots/min two launch rates, temperature rising ΔT at t_{pe} and t_{se} in three types rail, friction coefficient μ, and time t satisfy Poly 2D relationship.

In the light of obtaining lower maximal temperature in rail, ERL with convex rail is the best choice, and surface/channel cooling is better than channel cooling, launch rate 10 shots/min is more proper than 20 shots/min.

REFERENCES

[1] M. R. Doyle, D. J. Samuel, T. Conway, and R. R. Klimowski, "Electromagnetic aircraft launch system-EMALS," *IEEE Trans. Magn.*, vol. 31, no. 1, pp. 528–533, Jan. 1995.

[2] T. G. Engel and M. A. Prelas, "Asteroid mining and deflection using electromagnetic launchers," *IEEE Trans. Plasma Sci.*, vol. 45, no. 7, pp. 1327–1332, Jul. 2017.

[3] I. R. McNab, "Electromagnetic space launch considerations," *IEEE Trans. Plasma Sci.*, vol. 46, no. 10, pp. 3628–3633, Oct. 2018.

[4] H. Deng, Y. Wang, G. Fan, L. Liang, and Z. Yan, "Design and test of a single-stage double-layer multipole field electromagnetic launcher with a rotational performance," *IEEE Access*, vol. 7, pp. 112008–112014, 2019.

[5] H. Zhang, K. Dai, and Q. Yin, "Ammunition reliability against the harsh environments during the launch of an electromagnetic gun: A review," *IEEE Access*, vol. 7, pp. 45322–45339, 2019.

[6] Y. Zhang, J. Lu, S. Tan, B. Li, H. Wu, and Y. Jiang, "Heat generation and thermal management of a rapid-fire electromagnetic rail launcher," *IEEE Trans. Plasma Sci.*, vol. 47, no. 5, pp. 2143–2150, May 2019.

[7] S. Satapathy and C. Persad, "Thermal stresses in an actively cooled two-piece rail structure," *IEEE Trans. Magn.*, vol. 39, no. 1, pp. 468–471, Jan. 2003.

[8] H. Vanicek and S. Satapathy, "Thermal characteristics of a laboratory electromagnetic launcher," *IEEE Trans. Magn.*, vol. 41, no. 1, pp. 251–255, Jan. 2005.

[9] L. Jin, B. Lei, Q. Zhang, and R. Zhu, "Electromechanical performance of rails with different cross-sectional shapes in railgun," *IEEE Trans. Plasma Sci.*, vol. 43, no. 5, pp. 1220–1224, May 2015.

[10] F. Yang, Z. Zhao, Y. Liu, Y. Wu, Z. Chen, H. Sun, and M. Rong, "Electromagnetic-mechanical characteristics study of a high-speed electromagnetic launcher," *IEEE Trans. Plasma Sci.*, vol. 44, no. 10, pp. 2218–2225, Oct. 2016.

[11] A. N. Smith, R. L. Ellis, J. S. Bernardes, and A. E. Zielinski, "Thermal management and resistive rail heating of a large-scale naval electromagnetic launcher," *IEEE Trans. Magn.*, vol. 41, no. 1, pp. 235–240, Jan. 2005.

[12] D. A. Wetz, F. Stefani, and I. R. McNab, "Experimental results on a 7-m-Long plasma-driven electromagnetic launcher," *IEEE Trans. Plasma Sci.*, vol. 39, no. 1, pp. 180–185, Jan. 2011.

[13] R. Xu, D. Li, W. Zhao, W. Xu, W. Yuan, and P. Yan, "Research on insulation problems under multishot experiments in electromagnetic rail launcher," *IEEE Trans. Plasma Sci.*, vol. 45, no. 7, pp. 1353–1360, Jul. 2017.
[14] Q. Zhang, J. Li, S. Li, P. Liu, L. Jin, and G. Liu, "Causes of damage at electromagnetic Railgun's initial position and corresponding improvement measures," *IEEE Trans. Plasma Sci.*, vol. 47, no. 8, pp. 4184–4188, Aug. 2019.
[15] B. Tang, Q. Lin, and B. Li, "Research on thermal stress by current skin effect in a railgun," *IEEE Trans. Plasma Sci.*, vol. 45, no. 7, pp. 1689–1694, Jul. 2017.
[16] S. Fish, C. Phipps, and V. Tang, "Rail heating analysis for multishot EM gun operation," *IEEE Trans. Magn.*, vol. 35, no. 1, pp. 398–402, Jan. 1999.
[17] D. Motes, J. Keena, K. Womack, F. Stefani, and M. Crawford, "Thermal analysis of high-energy railgun tests," *IEEE Trans. Plasma Sci.*, vol. 40, no. 1, pp. 124–130, Jan. 2012.
[18] H. Li, B. Lei, Q.-A. Lv, and Z.-Y. Li, "Analysis on thermal character of interface between rail and armature for electromagnetic railgun," *IEEE Trans. Plasma Sci.*, vol. 41, no. 5, pp. 1426–1430, May 2013.
[19] S. Li, X. Wang, S. Zhang, L. Jin, and P. Liu, "Study on the lumped evaluation model of sliding electrical contact performance of railgun," *IEEE Trans. Plasma Sci.*, vol. 47, no. 5, pp. 2404–2411, May 2019.
[20] S. Li, J. Li, X. Wang, Q. Zhang, and P. Liu, "Research on segmentation evaluation model of sliding electrical contact performance of electromagnetic railgun," *IEEE Trans. Plasma Sci.*, vol. 47, no. 5, pp. 2424–2430, May 2019.
[21] P. Zuo, J. Li, X. Song, and J. Yuan, "Characteristics of current distribution in rails and armature with different section shape rails," *IEEE Trans. Plasma Sci.*, vol. 41, no. 5, pp. 1488–1492, May 2013.
[22] G. A. Shvetsov and S. V. Stankevich, "Three-dimensional numerical simulation of the joule heating of various shapes of armatures in railguns," *IEEE Trans. Plasma Sci.*, vol. 39, no. 1, pp. 456–460, Jan. 2011.
[23] X. Wan, J. Lou, J. Lu, and D. Liang, "Thermal analysis in electromagnetic launcher with different section shape rails," *IEEE Trans. Plasma Sci.*, vol. 46, no. 6, pp. 2091–2098, Jun. 2018.
[24] L. Brown, D. Xu, K. Ravi-Chandar, and S. Satapathy, "Coefficient of friction measurement in the presence of high current density," *IEEE Trans. Magn.*, vol. 43, no. 1, pp. 334–337, Jan. 2007.

XIAOBO WAN was born in Leshan, China. He received the B.S. degree in material physics and the M.S. degree in material physics and chemistry from Northwestern Polytechnical University, Xi'an, China, in 2004 and 2008, respectively. He is currently pursuing the Ph.D. degree in electrical engineering with Xi'an Jiaotong University, Xi'an. From 2008 to 2014, he was a Research and Development Engineer with the Western Superconducting Technologies, Xi'an. His current research interests include numerical calculation, optimal design of electrical devices, and superconducting electric power.

JUNYONG LU was born in Ezhou, China. He received the B.S. degree in electrical engineering from the Naval University of Engineering, Wuhan, China, in 2001, the M.S. degree from Xi'an Jiaotong University, Xi'an, China, in 2004, and the Ph.D. degree from the Naval University of Engineering, in 2010.

He is currently a Professor with the National Key Laboratory for Vessel Integrated Power System Technology, Wuhan. He is also the Chief Scientist of the National Defense Key Basic Research Program of China (973 Program). His current research interests include electromagnetic launch, energy storage, electrical devices, linear electric machine design, and its control.

Dr. Lu received the National Natural Science Funds for Outstanding Young Scholar, in 2015.

DELIANG LIANG was born in Dingxi, China. He received the B.S., M.S., and Ph.D. degrees in electrical engineering from Xi'an Jiaotong University, Xi'an, China, in 1989, 1992, and 1996, respectively. From 2001 to 2002, he was a Visiting Scholar with the Science Solution International Laboratory, Tokyo, Japan. Since 1999, he has been with the Department of Electrical Engineering, Xi'an Jiaotong University, where he is currently a Professor. His current research interests include optimal design, control, and simulation of electrical machines, and electrical machine technology in renewable energy.

JIANYONG LOU was born in Queshan, China. He received the B.S. and Ph.D. degrees in electrical engineering from Xi'an Jiaotong University, Xi'an, China, in 1999 and 2006, respectively. He is currently an Associate Professor with Xi'an Jiaotong University. His current research interests include special electrical machine and the numerical calculation of electrical devices.